Contribution from the Department of Chemistry, University of Iowa, Iowa City, Iowa 52242, and Nuclear Research Center, "Demokritos", Aghia Paraskevi, Attiki, Greece

Dinuclear Fe–Mo–S Complexes Containing the FeS_2Mo Core. Syntheses, Ground-State Electronic Structures, and Crystal and Molecular Structures of the $[(C_6H_5)_4P]_2[(C_6H_5S)_2FeS_2MoS_2]$, $[(C_2H_5)_4N]_2[(C_6H_5S)_2FeS_2WS_2]$, and $[(C_6H_5)_4P]_2[(S_5)FeS_2MS_2]$ (M = Mo, W) Complexes

D. COUCOUVANIS,* P. STREMPLE, E. D. SIMHON, D. SWENSON, N. C. BAENZIGER, M. DRAGANJAC, L. T. CHAN, A. SIMOPOULOS, V. PAPAEFTHYMIOU, A. KOSTIKAS, and V. PETROULEAS

Received March 5, 1982

The syntheses of the $(C_6H_5)_4P^+$ and $(C_2H_5)_4N^+$ salts of the $[(C_6H_5S)_2FeS_2MS_2]^{2-}$ and $[(S_5)FeS_2MS_2]^{2-}$ complex anions (M = Mo, W) are described in detail. The $[(C_6H_5)_4P]_2[(PhS)_2FeS_2MoS_2]$ salt (I) crystallizes in the monoclinic space group $P2_1/n$ with four molecules in the unit cell. The cell dimensions are a = 12.985 (7) Å, b = 20.926 (3) Å, c = 20.980 (7) Å, and β = 100.26 (2)°. The $(C_2H_5)_4N^+$ salt of the $[(C_6H_5S)_2FeS_2WS_2]^{2-}$ anion, II, crystallizes in the monoclinic space group $P2_1/c$ with four molecules in the unit cell. The cell dimensions for II are a = 10.9823 (8) Å, b = 10.7867 (9) Å, c = 30.981 (3) Å, and β = 97.35 (1)°. The $[(C_6H_5)_4P]_2[S_5FeS_2MS_2]$ complexes are X-ray isomorphous and isostructural and crystallize in the triclinic space group $P\bar{1}$ with two molecules in the unit cell. In addition the unit cell in both structures contains one molecule of dimethylformamide. For M = Mo (III), the unit cell dimensions are a = 11.874 (3) Å, b = 22.486 (5) Å, c = 19.698 (3) Å, α = 107.3 (1)°, β = 79.07 (3)°, and γ = 106.86 (4)°. For M = W (IV), the unit cell dimensions are a = 11.882 (7) Å, b = 22.487 (20) Å, c = 10.707 (7) Å, α = 106.989 (1)°, β = 78.929 (5)°, and γ = 107.159 (7)°. Intensity data for I–IV were collected with a four-circle computer-controlled diffractometer with use of the θ–2θ scan technique. In all structures, all non-hydrogen atoms were refined with anisotropic temperature factors and the hydrogen atoms were included in the structure factor calculations but not refined. Refinement by full-matrix least squares of 391 parameters on 5887 data for I, 343 parameters on 4580 data for II, 563 parameters on 2862 data for III, and 570 parameters on 3262 data for IV gave final R values of 0.059, 0.035, 0.087, and 0.082, respectively. The structures of the dinuclear complexes are described in terms of the edge-sharing MS_4 (M = Mo or W) and L_2FeS_2 tetrahedral units (L = PhS^- or $L_2 = S_5^{2-}$). A common characteristic in all structures is the nearly planar MS_2Fe rhombic core in which the M–Fe distances range from 2.737 (3) Å in III to 2.775 (1) Å in II. The Fe–S–M bridge angles in all complexes are found in the narrow range from 74.5 (3)° in I to 75.4 (3)° in II. Average values of selected structural parameters and the standard deviations from the mean are as follows. For I, Fe–S_b = 2.263 (3) Å, Fe–S_t = 2.297 (5) Å, Mo–S_t = 2.149 (6) Å, and Mo–S_b = 2.262 (9) Å; the range in S(i)–Fe–S(j) angles is 100.7 (1)–117.9 (1)° and in S(i)–Mo–S(j) angles is 105.5 (1)–112.2 (1)°. For II, Fe–S_b = 2.290 (3) Å, Fe–S_t = 2.306 (11) Å, W–S_t = 2.156 (3) Å, and W–S_b = 2.247 (10) Å; the range in S(i)–Fe–S(j) angles is 102.1 (1)–117.6 (1)° and in S(i)–W–S(j) angles is 105.8 (1)–110.5 (1)°. The distortions in the FeS_4 tetrahedra for I and II arise from intramolecular, phenyl ortho hydrogen–sulfur and metal interactions. For III and IV, Fe–S_b = 2.249 (3) and 2.269 (17) Å, Fe–S_t = 2.33 (3) and 2.322 (11) Å, Mo(W)–S_t = 2.15 (2) and 2.16 (2) Å, and Mo(W)–S_b = 2.260 (2) and 2.26 (2) Å. Ranges in S(i)–Fe–S(j) angles are 99.2 (2)–118.0 (3)° and 99.3 (3)–117.6 (4)° for III and IV, respectively. Ranges in S(i)–Mo(W)–S(j) are 104.7 (3)–112.4 (3)° and 105.3 (3)–112.1 (3)°. Angular distortions in the S_5FeS_2 tetrahedral units are attributed to packing forces. The Mössbauer spectra of I–IV have been studied as a function of temperature and an externally applied magnetic field. Values of the fine and hyperfine parameters and the magnetic moments are interpreted in terms of Fe(II) (S = 2) centers in all complexes. The values of the ^{57}Fe isomer shifts which are indicative of extensive Fe → S_2MS_2 charge transfer are slightly smaller for the WS_4^{2-} complexes than for the corresponding MoS_4^{2-} complexes. The less pronounced electron delocalization in the WS_4^{2-} complexes also is apparent in the electronic spectra and electrochemical properties of the complexes, which are discussed in detail.

Introduction

In the nitrogen-fixing nitrogenase enzymes,[1] the site for the catalytic reduction of dinitrogen to ammonia very likely is located within the Fe–Mo protein component of these complex enzymic systems. A minimal definition for the active site in nitrogenase, as an Fe–Mo–S aggregate, has emerged from the results of recent studies on the Fe–Mo protein. Outstanding among these results are (a) the isolation of a small-molecular-weight cofactor from the Fe–Mo protein that contains iron, all of the available molybdenum, and inorganic sulfide in an approximate (7 ± 1)/1/4 molar ratio,[2] (b) interpretation of the EPR and Mössbauer spectra of the Fe–Mo protein and of the cofactor in terms of a $S = {}^3/_2$ center that contains a molybdenum and about six iron atoms in a spin-coupled structure,[3] and (c) a detection by Mo-EXAFS (Mo X-ray absorption, fine-structure analyses) of approximately four sulfur atoms (at ~2.35 Å) and two or three iron atoms (at ~2.70 Å) around the Mo atom.[4]

Attempts toward the synthesis of heterometallic Fe–Mo–S complexes, in minimum structural compliance with the Mo-EXAFS results, have intensified in recent years. The basic approaches followed in the syntheses of these complexes employ MoS_4^{2-} and can be classified in two broad categories: (a) the spontaneous self-assembly reactions used extensively in the synthesis of the double cubanes with the $Mo_2Fe_6S_{11}$ framework[5] and derivative complexes[6] and (b) the MoS_4^{2-}–Fe(L)$_n$

* To whom correspondence should be addressed at the University of Iowa.

(1) (a) Eady, R. R.; Smith, B. E. In "A Treatise on Dinitrogen Fixation"; Hardy, R. W. F., Bottomley, F., Burns, R. C., Eds.; Wiley-Interscience: New York, 1979; Section II, Chapter 2. (b) Orme-Johnson, W. H.; Davis, L. C. In "Iron-Sulfur Proteins"; Lovenberg, W., Ed.; Academic Press: New York, 1977; Vol. 3, Chapter 2. (c) Stiefel, E. I. *Prog. Inorg. Chem.* **1977**, *22*, 1.

(2) (a) Shah, V. K.; Brill, W. J. *Proc. Natl. Acad. Sci. U.S.A.* **1977**, *74*, 3249. (b) Smith, B. E. In "Molybdenum Chemistry of Biological Significance"; Newton, W. E., Otsuka, S., Eds.; Plenum Press: New York, 1980; p 179.

(3) (a) Rawlings, J.; Shah, V. K.; Chisnell, J. R.; Brill, W. J.; Zimmermann, R.; Münck, E.; Orme-Johnson, W. H. *J. Biol. Chem.* **1978**, *253*, 1001. (b) Orme-Johnson, W. H.; Orme-Johnson, N. R.; Touton, L.; Emptage, M.; Henzl, M.; Rawlings, J.; Jakobson, K.; Smith, J. P.; Mims, W. B.; Huynh, B. H.; Münck, E.; Jacob, G. S. In "Molybdenum Chemistry of Biological Significance"; Newton, W. E., Otsuka, S., Eds.; Plenum Press: New York, 1979; p 85 and references therein.

(4) (a) Cramer, S. P.; Hodgson, K. O.; Gillum, W. O.; Mortenson, L. E. *J. Am. Chem. Soc.* **1978**, *100*, 3398. (b) Cramer, S. P.; Gillum, W. O.; Hodgson, K. O.; Mortenson, L. E.; Stiefel, E. I.; Chisnell, J. R.; Brill, W. J.; Shah, V. K. *Ibid.* **1978**, *100*, 3814.

0020-1669/83/1322-0293$01.50/0

ligand-exchange reactions used in the synthesis of simple Fe–Mo–S complexes containing the MoS_4 ligand.[7] In both of these approaches the syntheses of analogous Fe–W–S complexes (essential for comparative studies) have been accomplished with use of WS_4^{2-} in parallel reactions.

In previous communications we reported preliminary results on the synthesis, structural characterization, and electronic properties of various $[S_2MS_2FeL_2]^{2-}$ complexes (M = Mo, W; L = SPh^-,[8,9] Cl^-[10] or $L_2 = S_5^{2-}$[9]). Subsequent to our initial report on $(Et_4N)_2[(PhS)_2FeS_2MoS_2]$, Tieckelmann et al. reported on the synthesis and characterization of this molecule.[11] In addition reports on the $[Cl_2FeS_2MoS_2]^{2-}$ and $[Cl_2FeS_2WS_2]^{2-}$ anions appeared in the literature.[11-13]

In this paper we report in detail on the synthesis, electronic properties, and the crystal and molecular structures of the $(Ph_4P)_2[(PhS)_2FeS_2MoS_2]$, $(Et_4N)_2[(PhS)_2FeS_2WS_2]$, $(Ph_4P)_2[(S_5)FeS_2MoS_2]$, and $(Ph_4P)_2[(S_5)FeS_2WS_2]$ complexes. The structure determination of $(Ph_4P)_2[(PhS)_2FeS_2MoS_2]$ was undertaken in an attempt to interpret certain unusual structural and electronic characteristics of the $[(PhS)_2FeS_2MS_2]^{2-}$ anions (M = Mo, W) in the corresponding Et_4N^+ salts.

Experimental Section

Materials and Methods. Chemicals generally were used as purchased. Commercial grade dichloromethane (CH_2Cl_2) and acetonitrile (CH_3CN) were distilled from calcium hydride (CaH_2). Dimethylformamide (DMF) was dried over Linde 4A molecular sieves for 24 h and then distilled under reduced pressure at ~30 °C. Absolute ethanol and diethyl ether were used without any further purification. Most of the synthetic work was performed under anaerobic conditions with a Vacuum Atmospheres Dri-Lab and/or vacuum line techniques. The "inert" atmosphere gases (Ar, N_2) were purified by passing them through a H_2-reduced CuX ("De-ox") deoxygenation catalyst tower and immediately after through a sodium hydroxide pellet tower.

Synthesis. $(Ph_4P)_2[(PhS)_2FeS_2MoS_2]$. A solution of $(Ph_4P)_2[Fe(SPh)_4]$[14] (2.05 g, 1.75 mmol) in 15 mL of DMF was added to a solution of $(NH_4)_2MoS_4$[15] (0.45 g, 1.75 mmol) in 25 mL of DMF. The deep red solution that resulted was filtered through a medium-porosity glass fritted funnel after standing for ca. 5 min. To the filtrate was added 1 mL of absolute ethanol followed by diethyl ether to incipient crystallization. When the solution stood for ca. $^1/_2$ h, red-brown crystals formed and were isolated. The product was washed with several portions of diethyl ether and dried under vacuum.[16] An amount of 1.8 g of the complex was isolated (~87% yield); mp 155 °C dec.

Anal. Calcd for $FeMoS_6C_{60}H_{50}P_2$ (fw 1176.9): C, 61.18; H, 4.25; P, 5.26; S, 16.31; Fe, 4.74; Mo, 8.15. Found: C, 61.80; H, 4.41; P, 5.12; S, 15.51; Fe, 4.99; Mo, 7.28.

$(Et_4N)_2[(PhS)_2FeS_2MoS_2]$. This complex was obtained, in a manner analogous to that described for the corresponding Ph_4P^+ salt, in ~82% yield; mp 95 °C dec.

Anal. Calcd for $FeMoS_6C_{28}H_{50}N_2$ (fw 758.2): C, 44.3; H, 6.60; N, 3.70; S, 25.32; Fe, 7.36; Mo, 12.65. Found: C, 44.00; H, 6.57; N, 3.70; S, 24.53; Fe, 7.37; Mo, 12.68.

$(Ph_4P)_2[S_5FeS_2MoS_2]\cdot{}^1/_2DMF$. To a solution of $(Ph_4P)_2[(PhS)_2FeS_2MoS_2]$ (1.2 g, 1 mmol) in the minimum amount of DMF required for total dissolution was added a solution of dibenzyl trisulfide[17] $((C_7H_7S)_2S$; 2.84 g, 10 mmol) in 20 mL of DMF. The solution was stirred for ~15 min and filtered. To the filtrate was added 1 mL of absolute ethanol followed by diethyl ether to incipient crystallization.

After the solution stood for ca. $^1/_2$ h, dark brown crystals formed and were isolated: 1.0 g, 86% yield, mp ~160 °C dec.

Anal. Calcd for $FeMoS_9C_{48}H_{40}P_2\cdot{}^1/_2C_3H_7NO$ (fw 1155.7): C, 51.44; H, 3.80; N, 0.61; P, 5.36; S, 24.97; Fe, 4.83; Mo, 8.30. Calcd for $FeMoS_{9.3}C_{48}H_{40}P_2\cdot{}^1/_2C_3H_7NO$[18] (fw 1187.7): C, 51.01; H, 3.76; N, 0.60; P, 5.32; S, 25.56; Fe, 4.79; Mo, 8.23. Found: C, 50.62; H, 3.84; N, 0.64; P, 5.22; S, 24.23; Fe, 4.67; Mo, 8.43.

$(Ph_4P)_2[(PhS)_2FeS_2WS_2]$. To a light brown solution obtained by dissolving 0.997 g (0.851 mmol) of finely ground $(Ph_4P)_2Fe(SPh)_4$ in 20 mL of DMF was added with stirring a solution of 0.295 g (0.850 mmol) of freshly prepared $(NH_4)_2WS_4$[15b] in 10 mL of DMF. An instant color change to bright red was observed, and the solution was allowed to stir for 5 min. Following filtration, 2 mL of absolute ethanol was added and enough diethyl ether to incipient crystallization. After the solution stood, the red crystals that formed were isolated, washed twice with 10-mL portions of diethyl ether, and dried under vacuum. An amount of 0.78 g (0.62 mmol) of analytically pure product was obtained (76% yield).

Anal. Calcd for $FeWS_6C_{60}H_{50}P_2$ (fw 1264.8): C, 56.96; H, 3.98; S, 15.21; Fe, 4.41. Found: C, 56.92; H, 4.01; S, 15.09; Fe, 4.40.

$(Et_4N)_2[(PhS)_2FeS_2WS_2]$. Method A. The tetraethylammonium salt of $[(PhS)_2FeS_2WS_2]^{2-}$ was prepared in 85% yield in a manner analogous to that described for the Ph_4P^+ salt with $(Et_4N)_2Fe(SPh)_4$. The crystalline product is considerably less air stable than the Ph_4P^+ salt and oxidizes after brief exposures to air.

Method B. An amount of $(Et_4N)_2WS_4$[6a] (0.43 g, 0.751 mmol) was added to 25 mL of CH_3CN, and to this solution was added with stirring 0.22 g of KSPh (1.48 mmol). To the resulting suspension was added dropwise with stirring a solution of $Fe(ClO_4)_2\cdot6H_2O$ (0.20 g, 0.759 mmol) in 10 mL of CH_3CN over ca. 5 min. After 45 min of stirring the dark red solution was filtered whereby a white solid ($KClO_4$) was isolated and discarded. Diethyl ether was added slowly to the filtrate until the total volume of the solution was 200 mL. The crystalline product was isolated after ca. 2 h and washed with two 20-mL portions of diethyl ether. This material was recrystallized from CH_3CN solutions by adding diethyl ether to incipient crystallization. The final yield was 0.501 g, 79%.

Anal. Calcd for $FeWS_6C_{28}H_{50}N_2$ (fw 846.1): C, 39.71; H, 5.95; N, 3.30. Found: C, 39.44; H, 5.94; N, 3.26.

$(Ph_4P)_2[S_5FeS_2WS_2]\cdot{}^1/_2DMF$. An amount of 0.6 g (0.395 mmol) of $(Ph_4P)_2[(PhS)_2FeS_2WS_2]$ was dissolved into 10 mL of DMF. To this solution was added with stirring a solution of dibenzyl trisulfide (1.1 g, 3.95 mmol) in 10 mL of DMF. The resulting solution was warmed to ~80 °C for 5 min. A color change from red to red-brown was observed. The solution was filtered, allowed to cool to ambient temperature, and diluted with diethyl ether to incipient crystallization. After the solution stood for ~2 h a crystalline product formed and was isolated as a brown crystalline solid (0.44 g, 92% yield).

Anal. Calcd for $FeWS_9C_{48}H_{40}P_2\cdot{}^1/_2C_3H_7NO$ (fw 1243.6): C, 47.56; H, 3.54; N, 0.56; S, 23.32. Found: C, 46.75; H, 3.25; N, 0.41; S, 21.9.

Physical Measurements. Optical spectra were obtained on Cary Model 118 or 219 spectrophotometers. The infrared spectra of the complexes were obtained in Nujol mulls or KBr disks on a Beckman

(5) (a) Wolff, T. E.; Berg, J. M.; Warrick, C.; Hodgson, K. O.; Holm, R. H.; Frankel, R. B. *J. Am. Chem. Soc.* **1978**, *100*, 4630. (b) Christou, G.; Garner, C. D.; Mabbs, F. E. *Inorg. Chim. Acta* **1978**, *28*, L189. (c) Christou, G.; Garner, C. D.; Mabbs, F. E.; King, T. J. *J. Chem. Soc., Chem. Commun.* **1978**, 740. (d) Wolff, T. E.; Berg, J. M.; Power, P. P.; Hodgson, K. O.; Holm, R. H. *Inorg. Chem.* **1980**, *19*, 430 and references therein.

(6) (a) Wolff, T. E.; Power, P. P.; Frankel, R. B.; Holm, R. H. *J. Am. Chem. Soc.* **1980**, *102*, 4694. (b) Armstrong, W. H.; Holm, R. H. *Ibid.* **1981**, *103*, 6246 and references therein. (c) Wolff, T. E.; Berg, J. M.; Holm, R. H. *Inorg. Chem.* **1981**, *20*, 174.

(7) Coucouvanis, D. *Acc. Chem. Res.* **1981**, *14*, 201–209 and references therein.

(8) Coucouvanis, D.; Simhon, E. D.; Swenson, D.; Baenziger, N. C. *J. Chem. Soc., Chem. Commun.* **1979**, 361.

(9) Coucouvanis, D.; Baenziger, N. C.; Simhon, E. D.; Stremple, P.; Swenson, D.; Kostikas, A.; Simopoulos, A.; Petrouleas, V.; Papaefthymiou, V. *J. Am. Chem. Soc.* **1980**, *102*, 1730.

(10) Coucouvanis, D., et al. *J. Am. Chem. Soc.* **1980**, *102*, 1732.

(11) Tieckelmann, R. H.; Silvis, H. C.; Kent, T. A.; Huynh, B. H.; Waszczak, J. V.; Teo, B. K.; Averill, B. A. *J. am. Chem. Soc.* **1980**, *102*, 5550.

(12) Müller, A.; Tölle, H. G.; Bögge, H. *Z. Anorg. Allg. Chem.* **1980**, *471*, 115.

(13) Müller, A.; Sarkar, S.; Dommröse, A.-M.; Filgueira, R. *Z. Naturforsch., B: Anorg. Chem., Org. Chem.* **1980**, *35B*, 1592.

(14) Coucouvanis, D.; Swenson, D.; Baenziger, N. C.; Murphy, C.; Holah, D. G.; Sfarnas, N.; Simopoulos, A.; Kostikas, A. *J. Am. Chem. Soc.* **1981**, *103*, 3350.

(15) (a) Krüss, G. *Justus Liebigs Ann. Chem.* **1884**, *225*, 6. (b) Corleis, E. *Ibid.* **1886**, *232*, 244.

(16) Intensity indicators: s = strong; br = broad; m = medium; w = weak.

(17) Coucouvanis, D.; Kanatzidis, M.; Simhon, E.; Baenziger, N. C. *J. Am. Chem. Soc.* **1982**, *104*, 1874.

(18) This analysis is calculated after the detection of a $[(S_6)FeS_2MoS_2]^{2-}$ component in the crystal structure of the complex and is based on a mixture of 0.3/0.7 $(Ph_4P)_2[(S_6)FeS_2MoS_2]$–$(Ph_4P)_2[(S_5)FeS_2MoS_2]$.

Table I. Crystal and Refinement Data

	$[(C_6H_5)_4P]_2[(C_5H_5S)_2FeS_2MoS_2]$ (I)	$[(C_2H_5)_4N]_2[(C_6H_5S)_2FeS_2WS_2]$ (II)	$[(C_6H_5)_4P]_2[S_5FeS_2MoS_2]\cdot{}^1/_2DMF$ (III)	$[(C_6H_5)_4P]_2[S_5FeS_2WS_2]\cdot{}^1/_2DMF$ (IV)
fw	1176.9	846.75	1155.60	1243.51
a, Å	12.985 (7)	10.9823 (8)	11.874 (3)	11.882 (7)
b, Å	20.926 (3)	10.7867 (9)	22.486 (5)	22.487 (20)
c, Å	20.980 (7)	30.981 (3)	10.698 (3)	10.707 (7)
α, deg	90.00	90.00	107.3 (1)	106.99 (10)
β, deg	100.26 (2)	97.35 (1)	79.07 (3)	78.93 (5)
γ, deg	90.00	90.00	106.86 (4)	107.16 (7)
V, Å^3	5609.6	3639.9	2596.2	2596.6
Z	4	4	2	2
d_{calcd}	1.40	1.55	1.43	1.54
d_{obsd}	1.39[a]	1.54[a]	1.44[a]	1.55[a]
space group	$P2_1/n$	$P2_1/c$	$P\bar{1}$	$P\bar{1}$
cryst dimens, mm	0.60 × 0.6 × 0.7	0.06 × 0.26 × 0.59	0.2 × 0.04 × 0.03	0.1 × 0.2 × 0.04
μ, cm^{-1}	7.94	41.0	84.5	31.35
radiation	Mo[b]	Mo[b]	Cu[c]	Mo[b]
2θ limit, deg	45	50	100	40
unique reflctns	7327	6425	5327	4505
reflctns used, $F^2 > 3\sigma(F^2)$	5887	4580	2862	3262
variable parameters	391	343	563	570
R_1[d]	0.059	0.0352	0.0875	0.0815
R_2[e]	0.089	0.0421	0.1168	0.0978

[a] Determined by flotation in a CCl_4–pentane mixture. [b] Mo $K\alpha_1$ $\lambda = 0.709\,26$ Å. [c] Cu $K\alpha_1$ $\lambda = 1.5405$ Å. [d] $R_1 = \Sigma||\Delta F|/\Sigma|F_o||$. [e] $R_2 = [\Sigma w(\Delta F)^2/\Sigma w|F_o|^2]^{1/2}$.

IR-20A or Perkin-Elmer Models 21 and 421 spectrophotometers.

A Debye–Scherrer camera using nickel-filtered copper radiation was utilized to obtain X-ray powder diffraction patterns.[16] Proton NMR spectra were obtained on a Bruker HX-90E or JEOL FX90Q pulse FT NMR spectrometer with Me_4Si as internal standard. Chemical shifts are reported in parts per million (ppm). The following convention is used whenever isotropically shifted NMR is mentioned: a negative sign is assigned to a resonance appearing downfield from Me_4Si; a positive sign is given to an absorption occurring upfield from Me_4Si. This is directly opposite to the sign values printed by the spectrometer.

Electrochemical measurements were performed with a PAR Model 173 potentiostat/galvanostat and a PAR Model 175 universal programmer. The electrochemical cell consisted of platinum working and auxiliary electrodes. The reference electrodes were either the saturated calomel electrode (potential in volts vs. the standard hydrogen electrode: +0.241) or the $Ag/AgNO_3$ electrode with a potential vs. the saturated calomel electrode of +0.337 V. All solvents were properly dried and distilled, and tetra-*n*-butylammonium perchlorate (Bu_4NClO_4) was used as the supporting electrolyte. Normal concentrations used were ~0.001 M in complex and 0.1 M in supporting electrolyte. The cell was fitted with a bubbler through which purified N_2 or argon could be admitted for purging.

Mössbauer spectra were obtained in the temperature range of 1.2–300 K and in an external transverse magnetic field up to 6 T. A conventional constant-acceleration spectrometer was used for the measurements. The source was 100 mCi $^{57}Co(Rh)$ at room temperature. Magnetic susceptibility measurements were performed with a vibrating-sample magnetometer at temperatures between 2 and 300 K and in magnetic fields ranging up to 2 T. Absorbers were both powder samples and frozen solutions in DMF (dilute samples).

X-ray Diffraction Measurements. Collection and Reduction of Data. Specific details concerning crystal characteristics and X-ray diffraction methodology are shown in Table I. The crystals of the complexes were mounted on a Picker-Nuclear four-circle diffractometer automated by a DEC-PDP8-I computer with FACS-I-DOS software and equipped with a molybdenum-target X-ray tube (Mo $K\bar{\alpha}$, $\lambda = 0.7107$ Å),[19] a graphite monochromator ($2\theta_m = 12.20°$), crystal detector, and pulse height analyzer. For structures I, II, and IV reflections with 2θ values between 30 and 48° (Table I) were centered on the diffractometer and the preliminary cell dimensions were refined on the 2θ values of these reflections to yield the cell parameters shown in Table I. The diffraction peaks were measured by using a stepped θ–2θ scan data collection technique.[20]

The raw data were reduced to net intensities, estimated standard deviations were calculated on the basis of counting statistics, Lorentz polarization corrections were applied, and equivalent reflections were averaged. The estimated standard deviation of the structure factor was taken as the larger of that derived from counting statistics and that derived from scatter of multiple measurements. The least-squares program used minimizes $\sum w(\Delta|F|)^2$. The weighting function used throughout the refinements of the structures gives zero weight to those reflections with $F^2 \leq 3\sigma(F^2)$ and $w = 1/\sigma^2(F)$ to all others $[\sigma^2(F^2) = (pF^2)^2 + \sigma^2(F^2)$ (from counting statistics)].[21] The values of p are shown in Table I for each structure determination. The atomic scattering factors of the neutral atoms were used,[22] and all the scattering factors except those for hydrogen[23] were corrected by adding real and imaginary terms to account for the effects of anomalous dispersion.[24] Absorption corrections were applied by using the analytical program ABSORB,[25] which uses the analytical method of de Meulenaer and Tompa.[26]

The crystals used for data collection in all of the structure determinations were lodged in glass capillaries, and for each structure determination three standard reflections were measured after every 50 data points to monitor crystal and instrumental stability. Data were collected in the full sphere of the reciprocal space in all cases. Details concerning the extent of data collection in 2θ and space group information are shown in Table I.

Determinations of the Structures. $[(C_6H_5)_4P]_2[(C_6H_5S)_2FeS_2MoS_2]$ (I). Single crystals were obtained by the slow diffusion of diethyl ether into a pyridine solution of the compound. The details concerning data collection are outlined in Table I. A small change in the intensity of the three standard reflections ($0\bar{7}7$; $07\bar{7}$; $\bar{1}4,0,14$) was observed over the data collection period, and a correction was applied to the data (maximum correction factor 1.10). The data also were corrected for absorption ($\mu = 7.65$ cm^{-1}) with maximum and minimum corrections of 1.805 and 1.604, respectively. Of the 7327 unique reflections obtained 5887 had $F^2 > 3\sigma(F^2)$ and were used in the least-squares

(19) For the structure determination of $(Ph_4P)_2[(S_5)FeS_2MoS_2]$ *only*, a copper-target X-ray tube was used (Cu $K\bar{\alpha}$, $\lambda = 1.5405$ Å).

(20) Baenziger, N. C.; Foster, B. A.; Howells, M.; Howells, R.; Vander Valk, P.; Burton, D. J. *Acta Crystallogr., Sect. B* **1977**, *B33*, 2327.
(21) Grant, D. F.; Killean, R. C. G.; Lawrence, J. L. *Acta Crystallogr., Sect. B.* **1969**, *B25*, 374.
(22) Doyle, P. A.; Turner, P. S. *Acta Crystallogr., Sect. A* **1968**, *A24*, 390.
(23) Stewart, R. F.; Davidson, E. R.; Simpson, W. T. *J. Chem. Phys.* **1965**, *42*, 3175.
(24) Cromer, D. T.; Liberman, D. *J. Chem. Phys.* **1970**, *53*, 1891.
(25) The program ABSORB, modified for local use by F. J. Hollander, was taken from: Templeton, L.; Templeton, D. "Proceedings of the American Crystallographic Association Meeting"; American Crystallographic Association: Storrs, CT, 1973; Abstract E10, p 143.
(26) de Meulenaer, J.; Tompa, H. *Acta Crystallogr.* **1965**, *19*, 1014.

refinements. The positions of the Mo and Fe atoms were located in a Patterson synthesis map. Periodic structure factor calculations, Fourier syntheses, and location of new atoms in the electron density maps revealed the remaining 70 non-hydrogen atoms. Refinement of all non-hydrogen atoms with anisotropic temperature factors converged to $R_1 = 0.072$ and $R_2 = 0.120$. At this stage the 50 hydrogen atoms were included in the structure factor calculations at their calculated positions (C–H = 0.95 Å) but were not refined. The final values for the residuals R_1 and R_2 after convergence were 0.059 and 0.089, respectively. A final difference Fourier synthesis did not show electron density maxima higher than ~0.3 e Å^{-3}.

$[(C_2H_5)_4N]_2[(C_6H_5S)_2FeS_2WS_2]$ (II). Single crystals were obtained by the slow diffusion of diethyl ether into a DMF solution of the compound. The X-ray powder pattern of the crystals was virtually identical with that of the analogous Mo compound. The details of the data collection are outlined in Table I. A slow decrease in the intensity of the three standard reflections (600; 0,0,22; 0$\bar{6}$0) was observed over the data collection period, and the data were corrected by a standard "fix-up" program with a maximum correction factor of 1.32. The data were corrected for absorption ($\mu = 41.04$ cm^{-1}) with maximum and minimum corrections of 2.769 and 1.268 respectively. Of the 6425 unique reflections obtained, 4580 had $F^2 > 3\sigma(F^2)$ and were used in the least-squares refinements.

Atomic coordinates from the Mo analogue,[8,11] for the 38 non-hydrogen atoms, were input in the least-squares calculations and refined with anisotropic temperature factors. Refinement converged to $R_1 = 0.043$ and $R_2 = 0.058$. At this point the hydrogen atoms were included at their calculated positions (0.95 Å from the appropriate carbon atoms) with temperature factors equal to the mean value of the carbon atom temperature factors. The hydrogen atoms were used in the structure factor calculation but were not refined. The final values for R_1 and R_2 after convergence were 0.035 and 0.042, respectively.

$[(C_6H_5)_4P]_2[(S_5)FeS_2MS_2]\cdot{}^1/_2HCON(CH_3)_2$ (M = Mo (III), W (IV)). Single crystals of both complexes were obtained by the slow diffusion of diethyl ether into DMF solutions of the complexes. The powder patterns for the Mo and W complexes are virtually identical. The details of the data collection are outlined in Table I. No decrease in the intensities of the standard reflections was observed for either of the two structures. The data for both crystals were corrected for absorption. From the corrected data for the Mo complex a Patterson synthesis revealed the positions of the Mo, Fe, and four S atoms. Successive electron density maps yielded the positions of all non-hydrogen atoms of the anion, the cation, and the disordered $HCON(CH_3)_2$ molecule (N atom at $^1/_2$, $^1/_2$, 0). Isotropic refinement of all non-hydrogen atoms converged to R_1 and R_2 values of 0.120 and 0.135, respectively. Further refinement with anisotropic temperature factors for all non-hydrogen atoms (except those for the disordered DMF molecule) converged to R_1 and R_2 values of 0.095 and 0.120, respectively. At this stage our results were communicated.[9] The positions of the 47 hydrogen atoms were calculated (C–H at 0.95 Å) and included in the structure factor calculation but not refined. A difference Fourier synthesis at this stage revealed two weak electron density maxima around the S_5 chelated ring. An evaluation of the positions of these maxima showed that the site of the S_5 fragment was occupied also by an S_6 fragment as a minor component in such a way that the two fragments had four sulfur atoms in common. The minor S_6 fragment contributed the two new maxima in the electron density map. These two maxima were located on either side of the fourth S atom (S(9)) in the S_5 unit. Two new sulfur atoms (S(9′) and S(10)) were introduced at ~0.3 occupancy, and the occupancy of the S(9) atom in the S_5 unit was reduced to ~0.7. The close proximity of S(9), S(9′), and S(10) and the small occupancy factors of S(9′) and S(10) dictated that these atoms as well as the neighboring S(2) and S(8) atoms were refined with isotropic temperature factors. A number of refinements with different relative occupancy factors (0.3 ± 0.1 and 0.7 ∓ 0.1) showed a shallow minimum in R_2 for occupancy factors of 0.3 and 0.7. The 0.3 and 0.7 values also are in agreement with the Mössbauer data, which indicated two iron-containing components with these relative weights. In the final refinement R_1 and R_2 were 0.087 and 0.117, and in the final difference Fourier map no peaks higher than ~0.6 e Å^{-3} were found.

The final coordinates obtained from the structure of the Mo complex were used as an input for refinement of the W analogue. Refinement on the latter with anisotropic temperature factors for all non-hydrogen atoms (except for the disordered DMF molecule) converged to R_1 and R_2 of 0.089 and 0.109, respectively. Introduction of the 47 hydrogen atoms at their calculated positions in the structure factor calculations reduced R_1 and R_2 to 0.081 and 0.098. A final difference Fourier showed no indications of a S_6 minor component and no peaks higher than 0.4 e Å^{-3}. It should be noted that only one quadrupole doublet is observed in the Mössbauer spectrum of this compound, consistent with the absence of a minor S_6 component.

Crystallographic Results. The final atomic positional and thermal parameters for $(Ph_4P)_2[(PhS)_2FeS_2MoS_2]$, $(Et_4N)_2[(PhS)_2FeS_2WS_2]$, and $(Ph_4P)_2[(S_5)FeS_2MoS_2]\cdot{}^1/_2DMF$, with standard deviations derived from the inverse matrices of the least-squares refinements, are compiled in Tables II, III, and IV, respectively. The corresponding data for $(Ph_4P)_2[(S_5)FeS_2WS_2]\cdot{}^1/_2DMF$ (isomorphous and isostructural to the Mo analogue) have been deposited as supplementary material. Intramolecular distances and angles for the anions in all structures are given in Table V. The atom-labeling schemes are shown in Figures 1 and 2. Stereoviews of crystal packing have been deposited as supplementary materials.

The generated atomic parameters of the hydrogen atoms have been deposited together with tables of the observed values of F, their esd's, and the $|F_o| - |F_c|$ values. A table of the angular distortions and intramolecular H contacts of the FeS_4 units in the $C_2[(PhS)_2FeS_2MS_2]$ lattices is also deposited. (See paragraph at the end of this paper regarding supplementary material.)

Results and Discussion

Synthesis of the $[L_2FeS_2MS_2]^{2-}$ Complexes (L = SPh^-, M = Mo, W; L = S_5^{2-}, M = Mo, W). The $[(PhS)_2FeS_2MS_2]^{2-}$ complex anions are obtained in excellent yield by the reactions of the $[Fe(SPh)_4]^{2-}$ complex[14] with the NH_4^+ salts of the tetrathiometalate anions (MS_4^{2-}, M = Mo, W). The simple substitution reaction of two PhS^- ligands in the coordination sphere of the $Fe(SPh)_4^{2-}$ complex by the bidentate, chelating MS_4^{2-} ligands is analogous to the reaction employed in the synthesis of the $[(PhS)_2Fe(Dts)]^{2-}$ complexes[27] (Dts = the dithiosquarate ligand, $S_2C_4O_2^{2-}$).

The $[(S_5)FeS_2MS_2]^{2-}$ complexes are obtained by the reaction of an excess of the aliphatic trisulfide $(C_7H_7)_2S_3$ with the $[(PhS)_2FeS_2MS_2]^{2-}$ complexes in DMF solution. This reaction is similar to the reaction of the $[(PhS)_2FeS_2Fe(SPh)_2]^{2-}$ anion with $(C_7H_7)_2S_3$ to give[28] $[(S_5)FeS_2Fe(S_5)]^{2-}$. The generation of the S_5^{2-} ligand in reactions of the trisulfide $(C_7H_7)_2S_3$ with terminally bound PhS^- ligands very likely involves oxidation of the PhS^- ligands by S_5^0 fragments generated from the aliphatic trisulfide. A possible mechanism for the generation of S^0 and S_x^0 fragments, in solutions containing thiophenolate complexes and the trisulfides RSSSR, is similar to the one proposed (Scheme I) for the RS^--catalyzed dissociation of thiocystine.[29] The S^0 atoms can serve as two-electron oxidizing

Scheme I

$$RSSSR + R'S^- \rightleftarrows RSS^- + R'SSR$$

$$RSS^- \rightarrow RS^- + S^0$$

$$RS^- + R'SSR \rightleftarrows RSSR + R'S^-$$

$$\text{or } RSSSR + R'S^- \rightarrow RSSR + R'S^- + S^0$$

agents with the concomitant generation of the S^{2-} as observed[28] in the reaction

$$2Fe^{II}(SPh)_4^{2-} + 2RSSSR \rightarrow (PhS)_2Fe^{III}S_2Fe^{III}(SPh)_2^{2-} + 2RSSR$$

In the presence of excess RSSSR, higher order polysulfides are expected to form by the reactions

$$RSSSR + S^0 \rightarrow RSSSSR$$

$$RS(S)_xSR + S^0 \rightarrow RS(S)_{x+1}SR$$

(27) Holah, D. G.; Coucouvanis, D. *J. Am. Chem. Soc.* **1975**, *97*, 6917.
(28) Coucouvanis, D.; Swenson, D.; Stremple, P.; Baenziger, N. C. *J. Am. Chem. Soc.* **1979**, *101*, 3392.
(29) Abdolrasulnia, R.; Wood, J. L. *Bioorg. Chem.* **1980**, *9*, 253.

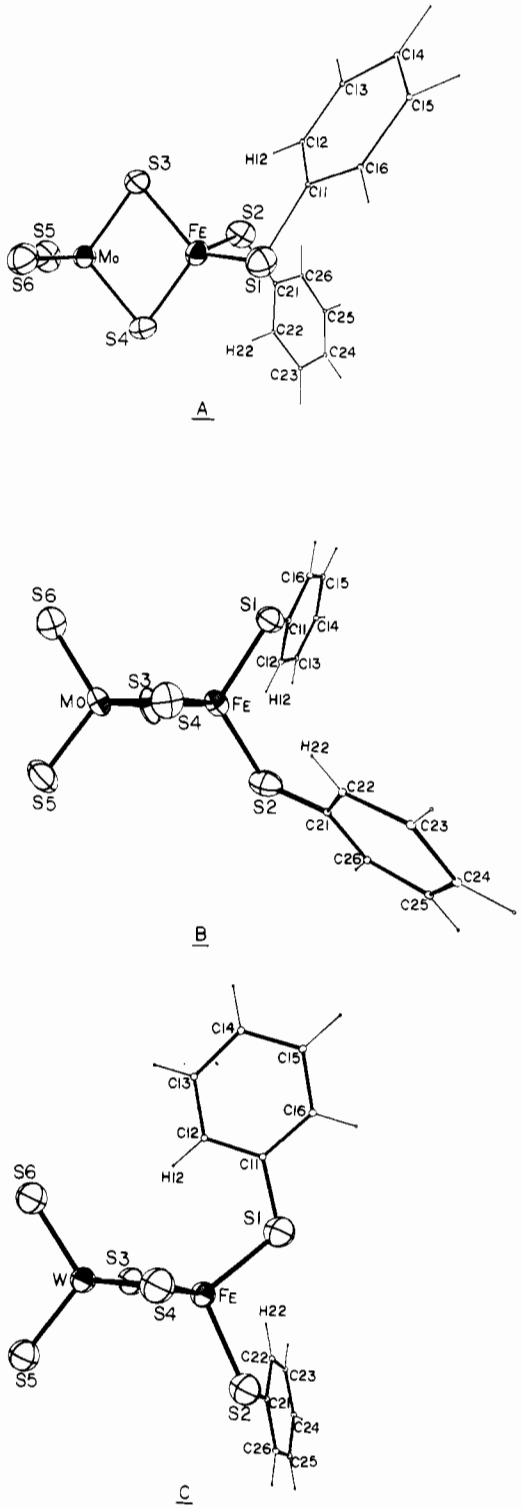

Figure 1. Atom-labeling and -numbering scheme for two views of the $[(PhS)_2FeS_2MoS_2]^{2-}$ anion in $(Ph_4P)_2[(PhS)_2FeS_2MoS_2]$ (A, B) and for the $[(PhS)_2FeS_2WS_2]^{2-}$ anion in $(Et_4N)_2[(PhS)_2FeS_2WS_2]$ (C). Thermal ellipsoids as drawn by ORTEP (Johnson, C. K. *Oak Ridge Natl. Lab. [Rep.] ORNL (U.S.)* **1965**, ORNL-3794) represent the 50% probability surfaces.

A repetition of Scheme I is expected to generate S_x^0 fragments, including S_5^0, which could serve as oxidizing agents for the $(PhS)_2FeL_2$ complexes according to the reaction

$$(PhS)_2FeL_2 + S_5^0 \rightarrow (S_5)FeL_2 + PhSSPh$$

Oxidation of the $[(PhS)_2FeS_2MS_2]^{2-}$ complexes by lower order S_x^0 fragments cannot be ruled out; however, we have been unable to isolate products containing the S_x^{2-} "chelating" ligands (x = 2–4). Apparently, the superior thermodynamic

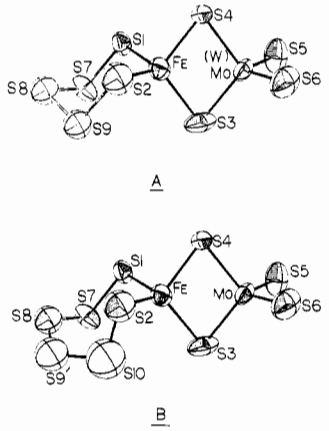

Figure 2. Atom-labeling and -numbering schemes of the $[(S_5)FeS_2MS_2]^{2-}$ anions (M = Mo, W) (A) and the $[(S_6)FeS_2MoS_2]^{2-}$ minor component in the structure of the molybdenum analogue (B). Thermal ellipsoids as drawn by ORTEP represent the 50% probability surfaces.

stability of the S_5Fe ring accounts for the preferential formation of the S_5^{2-} ligand. A minor product that is obtained in the synthesis of the $(Ph_4P)_2[(S_5)FeS_2MoS_2]$ complex is the $[(S_6)FeS_2MoS_2]^{2-}$ anion, which cocrystallizes as a minor component. In the crystal structure of $(Ph_4P)_2[(S_5)FeS_2MoS_2]$ (vide infra) approximately 30% of the anion lattice site is occupied by the $[(S_6)FeS_2MoS_2]^{2-}$ anion. We were unable to detect a similar minor component in the structure of the isostructural W analogue complex.[30]

Infrared Spectra. The tetrahedral tetrathiometalate anions MS_4^{2-} have one infrared-active stretching mode, and this is the triply degenerate T_2 mode (ν_3). The totally symmetric A_1 mode is infrared inactive and Raman active. In MoS_4^{2-} ν_3 is observed as a strong band at 480 cm^{-1}; the corresponding vibration in WS_4^{2-} is found at 458 cm^{-1}. The A_1 mode (ν_1) vibration can be observed as a weak band in the infrared spectra at 460 cm^{-1} for the MoS_4^{2-} anion and at 484 cm^{-1} for the WS_4^{2-} anion.[31] The presence of the ν_1 vibration in the infrared spectra probably is due to distortions of the MS_4^{2-} anions from ideal T_d symmetry, due to environmental lattice effects. In the $[(PhS)_2FeS_2MS_2]^{2-}$ and $[(S_5)FeS_2MS_2]^{2-}$ complexes, where the coordinated MS_4 unit has C_{2v} symmetry, the T_2 mode is expected to reduce into A_1, B_1, and B_2 modes, all of which are infrared active. Similarly the infrared-inactive A_1 mode (in T_d symmetry) becomes infrared active in C_{2v} symmetry. A total of four stretching vibrations therefore are expected for the coordinated MS_4^{2-} anions in the $Fe–S_2MS_2$ complexes. In the infrared spectra of the $[(PhS)_2FeS_2MoS_2]^{2-}$ and $[(S_5)FeS_2MoS_2]^{2-}$ anions, bands at 498, 484, and 444 cm^{-1} for the former and 503, 487, and 441 cm^{-1} for the latter are observed. The low-energy bands at 441 and 444 cm^{-1} very likely are associated with Mo–S vibrations involving the bridging S atoms. The high-energy bands are associated with the terminal Mo–S atoms.[32] The observation of only three Mo–S vibrations in the spectra very likely reflects insufficient resolution of two vibrations of very similar energies. Similar assignments have been made for the Mo–S vibrations of the coordinated MoS_4^{2-} anion in the $[Ni(MoS_4)_2]^{2-}$ complex, in which all of the expected four vibrational frequencies can be resolved.[33]

(30) Synthetic efforts currently in progress are aimed toward the isolation of pure $[(S_x)FeS_2MS_2]^{2-}$ complexes, x = 4–6.
(31) Diemann, E.; Müller, A. *Coord. Chem. Rev.* **1973**, *10*, 79.
(32) Paulet-Boschen, I.; Krebs, B.; Müller, A.; Koniger-Ahlborn, E.; Dornfeld, H.; Schulz, H. *Inorg. Chem.* **1978**, *17*, 1440.
(33) (a) Müller, A.; Diemann, E.; Heinsen, H.-H. *Chem. Ber.* **1971**, *104*, 975. (b) Müller, A.; Ahlborn, E.; Heinsen, H.-H. *Z. Anorg. Allg. Chem.* **1971**, *386*, 102.

In the infrared spectra of the $[(PhS)_2FeS_2WS_2]^{2-}$ and $[(S_5)FeS_2WS_2]^{2-}$ complexes the W–S vibrational frequencies are found at 487, 481, 441, and 432 cm^{-1} in the former and at 485 br, 446, and 437 cm^{-1} in the latter.

Structures. (A) $C_2[(SPh)_2FeS_2MS_2]$ Complexes (M = Mo, W; C = Et_4N^+, Ph_4P^+). The Mo and W complexes with a common counterion are isomorphous and isostructural. The $[(SPh)_2FeS_2MS_2]^{2-}$ anions (Figure 1) in the two different unit cells of the Et_4N^+ and Ph_4P^+ salts show many similarities and certain important differences. In the Et_4N^+ structure the anions are closer to each other and the shortest *interionic* Fe–Mo(W), Fe–Fe, and Mo(W)–Mo(W) distances are 9.070 (9.071), 8.487 (8.477), and 9.624 (9.635) Å.[34] In the Ph_4P^+ structure the nearest interionic Fe–Mo, Fe–Fe, and Mo–Mo distances are 9.702, 9.919, and 9.265 Å, respectively. The relatively shorter Fe–Fe interionic distances in the Et_4N^+ salts may account for the magnetic interactions apparent at low temperatures in the magnetically perturbed Mössbauer spectra of the $[(PhS)_2FeS_2MoS_2]^{2-}$ complex in the Et_4N^+ salt.[11] Such interactions are not observed for the Ph_4P^+ salts of the complexes or for the Et_4N^+ salt (M = Mo) in solution[11] (vide infra).

The basic $S_2FeS_2MS_2$ core structure in the $[(PhS)_2FeS_2MS_2]^{2-}$ anions (Figure 1) can be described in terms of two edge-sharing FeS_4 and MS_4 tetrahedral units. In all structures the coordinated MS_4 anions (M = Mo, W) show the effects of charge delocalization, brought about by chelation to the Fe atoms. Thus short M–S terminal bond lengths and comparatively longer M–S bridging bond lengths are observed (Table V). The mean value of all Mo–S bonds[35] in the coordinated MoS_4 anions in the Et_4N^+ and Ph_4P^+ salts is 2.201 Å. This value is somewhat longer than the Mo–S bond length in $(Et_4N)_2MoS_4$, 2.176 (5) Å,[36] and marginally supports a partial reduction of the MoS_4 units as a result of $FeS_4 \rightarrow MoS_4$ charge transfer.

The $\overline{W-S}$ bond length in $(Et_4N)_2[(PhS)_2FeS_2WS_2]$ at 2.201 Å[35] also shows a slight lengthening when compared to that of the W–S bond in WS_4^{2-} at 2.17 (1) Å.[37] The S–M–S angles in the coordinated MS_4 anions are close to the ideal tetrahedral value of 109.49° (range 104.7–112.4°).

The Fe–S bond lengths in the FeS_4 units (Table V) can be divided into two pairs for all of the $[(PhS)_2FeS_2MS_2]^{2-}$ anions. For M = Mo the terminal Fe–S bond lengths have a mean value[35] of 2.310 (7) Å. The corresponding value in the W analogue is 2.306 (8) Å. By comparison the mean value of the bridging Fe–S bond lengths is 2.257 (9) Å for M = Mo[35] and 2.290 (2) Å for M = W. The longer bridging Fe–S bond lengths in $[(PhS)_2FeS_2WS_2]^{2-}$ suggest that the WS_4^{2-} anion is not as strongly bound to the iron atom as the MoS_4^{2-} anion. An evaluation of the relative bridge strengths in the $[(PhS)_2FeMS_4]^{2-}$ complexes can be obtained from a correlation of the differences, $(\overline{Fe-S}) - (\overline{Fe-S_t})$ and $(\overline{Fe-S}) - (\overline{Fe-S_b})$. In the calculation of these differences for each anion $\overline{Fe-S}$, $\overline{Fe-S_t}$, and $\overline{Fe-S_b}$ are the mean values of the Fe–S bonds for all sulfur atoms, the terminal sulfur atoms, and the bridging sulfur atoms, respectively. In such a correlation[10] larger positive values for $(\overline{Fe-S}) - (\overline{Fe-S_b})$ and larger negative values fof $(\overline{Fe-S}) - (\overline{Fe-S_t})$ are considered as indicative of a stronger FeS_2M bridging unit. For the $[(PhS)_2FeS_2MoS_2]^{2-}$ complexes ($\overline{Fe-S}$ = 2.283 Å) the differences are 0.027 (8) and −0.027 (8) Å. In the $[(PhS)_2FeS_2WS_2]^{2-}$ complex ($\overline{Fe-S}$ = 2.298 Å) the corresponding values are 0.008 (8) and −0.008 (8) Å. Weaker $Fe-S_2MS_2$ interactions for M = W vs. M = Mo in all of the $[L_2FeS_2MS_2]^{2-}$ complexes also are suggested by the ^{57}Fe Mössbauer spectra of these complexes (vide infra).

The FeS_4 units in the $[(PhS)_2FeS_2MS_2]^{2-}$ complexes are distorted significantly from the ideal T_d symmetry. The origin of these distortions is the same as the one identified and analyzed for the $M(SPh)_4^{2-}$ complexes.[14] In the tetrahedral thiophenolate complexes the M–S bonds in the M–S–Ph units are very nearly coplanar with the attached phenyl rings.[38] The most stable orientations of the S–Ph units are those where the phenyl rings are orthogonal to and approximately bisect the S–S edge of the MS_4 tetrahedra. There exist three equivalent orientations for each phenyl ring, which are related by the threefold axis that passes through the M–S bond to which the phenyl ring is attached.

The conformations of the phenyl rings in the Ph_4P^+ and Et_4N^+ salts of the $[(PhS)_2FeS_2MS_2]^{2-}$ anions are different. However, for the anion of the Ph_4P^+ salt (Figure 1A) a clockwise rotation of the S(2)–phenyl ring 2 unit about the Fe–S(2) bond by 120° and a counterclockwise rotation of the S(1)–phenyl ring 1 unit about the Fe–S(1) bond by 120° will result in a conformation that is virtually identical with that of the $[(PhS)_2FeS_2MS_2]^{2-}$ anions in the Et_4N^+ salts (Figure 1C).

The location of the ortho hydrogens (H(12) and H(22), Figure 1) in close proximity to the sulfur atoms[39] accounts for the systematic distortions of the FeS_4 units from ideal tetrahedral symmetry.

Repulsions between H(12) and S(2), S(3) (Figure 1A,B) result in S(1)–Fe–S(2) and S(1)–Fe–S(3) angles greater than 109° and a S(1)–Fe–S(4) angle smaller than 109°. Additional evidence for these repulsions is apparent in the S(1)–C(11)–C(12) and S(1)–C(11)–C(16) angles. The former is greater than 120° while the latter is smaller than 120° (see footnote *c* in Table V).

An examination of the interactions between the other ortho-hydrogen atoms and the appropriate sulfur atoms (H(22)–S(4), Figure 1A,B; H(12)–S(3) and H(22)–S(1), Figure 1C) shows identical distortions for the corresponding S–Fe–S and S–C–C angles. Essentially the same distortions are apparent for the anion in $(Et_4N)_2[(PhS)_2FeS_2MoS_2]$.[8,11]

As observed in the structures of the tetrahedral $M(SPh)_4^{2-}$ anions, each of the proximal ortho hydrogens (H(11) and H(22) (Figure 1)) in the structures of the $[(PhS)_2FeS_2MS_2]^{2-}$ complexes is closer to one of the S atoms than to the other.[39] As suggested previously, the ortho-hydrogen atoms choose one of the two local minima of van der Waals interaction energy between the metal and the appropriate sulfur atoms (see also Figure 7 of ref 14).

(34) For the Mo complexes values were obtained from ref 8 and 11.

(35) The data reported in ref 8 and 11 were averaged out. Throughout this paper the standard deviations of the averages are taken as the larger of the individual standard deviations or the standard deviation from the mean $\sigma = [\sum_0^N((X_i - \bar{X})^2/(N-1))]^{1/2}$. The mean values of the M–S and Fe–S bonds in the coordinated MS_4^{2-} (M = Mo, W) and "FeS_4" units have been obtained by averaging chemically nonequivalent bonds. These values in reality represent the centroids of the distribution of M–S or Fe–S bond lengths. The spread in this distribution is mostly a measure of the range of variation of the M–S or Fe–S *bond orders* rather than a measure of error in bond length measurements. The bond order–bond length curve is not linear; however for small variations in bond order, the centroid (mean) of the bond distances in symmetrically bonded species should not differ by more than a few thousandths of an angstrom from the mean of an asymmetrically bonded species. When significant differences are present, they may arise from small changes in the oxidation state of the central (M or Fe) atom.

(36) Kanatzidis, M.; Coucouvanis, D., submitted for publication.

(37) Sasvari, K. *Acta Crystallogr.* **1963**, *16*, 719.

(38) A possible reason for the preferred planar binding of the S–Ph ligands is a π type of interaction by the S atom lone-pair electrons and the aromatic π system. An ab initio calculation of phenol (Richards, R.; Walker, S.; Hinkley, T. *J. Am. Chem. Soc.* **1972**, *94*, 1496) shows the totally planar configuration, 5 kcal/mol lower in energy than the configuration with the C–O–H plane perpendicular to the benzene ring.

(39) Close intermolecular contacts: $(Ph_4P)_2[(PhS)_2FeS_2MoS_2]$, S(4)–H(22) 3.00 Å, S(2)–H(12) 3.00 Å, S(3)–H(12) 3.23 Å; $(Et_4N)_2[(PhS)_2FeS_2WS_2]$, S(1)–H(22) 2.95 Å, S(3)–H(12) 3.14 Å.

Table II. Positional and Thermal Parameters and Their Standard Deviations in the Compound $[(C_6H_5)_4P]_2[(C_6H_5S)_2FeS_2MoS_2]$[a]

atom	x	y	z	B_{11}	B_{22}	B_{33}	B_{12}	B_{13}	B_{23}
Mo	0.48313 (4)	0.27892 (2)	0.50358 (3)	4.75 (3)	3.54 (3)	4.22 (3)	0.67 (2)	1.87 (2)	0.25 (2)
Fe	0.50852 (7)	0.21194 (4)	0.39526 (4)	4.15 (5)	3.69 (4)	4.60 (5)	0.59 (3)	1.31 (3)	−0.16 (3)
S(4)	0.4897 (1)	0.17123 (8)	0.49257 (9)	6.3 (1)	3.64 (7)	5.54 (9)	−0.21 (6)	1.48 (7)	0.56 (6)
S(3)	0.4985 (2)	0.31912 (8)	0.4060 (1)	10.2 (1)	3.82 (8)	5.8 (1)	1.72 (8)	3.8 (1)	0.77 (7)
S(6)	0.6148 (2)	0.31171 (9)	0.5724 (1)	6.3 (1)	5.06 (9)	6.3 (1)	−0.63 (7)	1.82 (8)	−0.25 (7)
S(5)	0.3365 (2)	0.3070 (1)	0.5295 (1)	5.9 (1)	8.9 (1)	7.5 (1)	1.87 (9)	2.92 (9)	−0.5 (1)
S(1)	0.6705 (1)	0.17943 (8)	0.37924 (8)	4.18 (7)	4.74 (8)	4.91 (8)	0.80 (6)	0.76 (6)	0.06 (6)
S(2)	0.3756 (1)	0.1948 (1)	0.3084 (1)	4.26 (8)	7.1 (1)	6.1 (1)	0.80 (7)	0.24 (7)	0.81 (8)
C(11)	0.7027 (5)	0.2208 (3)	0.3099 (3)	4.2 (3)	3.8 (3)	5.4 (4)	0.1 (2)	0.7 (3)	−0.8 (2)
C(12)	0.6325 (6)	0.2568 (4)	0.2674 (4)	5.4 (4)	6.3 (4)	7.6 (5)	1.9 (3)	2.8 (3)	1.3 (4)
C(13)	0.6599 (9)	0.2832 (4)	0.2132 (5)	9.6 (7)	8.1 (6)	8.7 (6)	2.2 (4)	3.9 (5)	3.9 (4)
C(14)	0.7602 (7)	0.2770 (4)	0.2007 (5)	6.4 (5)	7.2 (5)	9.7 (6)	−0.3 (4)	3.4 (5)	2.7 (4)
C(15)	0.8316 (6)	0.2429 (5)	0.2442 (5)	4.7 (4)	7.9 (5)	8.5 (5)	−1.2 (4)	2.2 (4)	−0.2 (4)
C(16)	0.8027 (6)	0.2152 (3)	0.2975 (4)	3.9 (3)	6.2 (4)	6.5 (4)	−0.5 (3)	0.2 (3)	0.4 (3)
C(21)	0.3438 (5)	0.1139 (4)	0.2980 (4)	2.4 (3)	8.0 (4)	5.7 (4)	0.2 (3)	1.0 (3)	−1.6 (3)
C(22)	0.3829 (5)	0.0673 (4)	0.3438 (4)	3.9 (3)	6.0 (4)	6.6 (4)	−0.3 (3)	1.6 (3)	−1.1 (3)
C(23)	0.3529 (7)	0.0027 (4)	0.3337 (5)	5.9 (4)	7.0 (5)	9.7 (6)	−0.5 (4)	4.9 (5)	−0.3 (4)
C(24)	0.2825 (8)	−0.0144 (5)	0.2799 (7)	4.0 (4)	9.5 (7)	14.1 (10)	−2.3 (4)	4.5 (5)	−6.0 (7)
C(25)	0.2425 (7)	0.0307 (7)	0.2356 (6)	3.5 (4)	14.0 (10)	11.0 (8)	−0.6 (5)	1.2 (4)	−7.4 (7)
C(26)	0.2722 (6)	0.0948 (5)	0.2441 (4)	3.8 (3)	10.4 (6)	6.9 (5)	0.2 (4)	0.7 (3)	−2.1 (4)
P(A)	0.0204 (1)	−0.00087 (7)	0.65156 (8)	3.96 (7)	4.53 (7)	4.28 (7)	0.85 (5)	1.14 (6)	0.76 (5)
P(B)	0.0399 (1)	0.42360 (7)	0.37338 (7)	3.47 (6)	3.96 (7)	4.34 (7)	0.30 (5)	1.15 (5)	0.26 (5)

atom	x	y	z	B	atom	x	y	z	B
C(A1)	0.0405 (5)	−0.0158 (3)	0.7379 (3)	4.1 (1)	C(B1)	0.0536 (4)	0.3711 (3)	0.3075 (3)	3.7 (1)
C(A2)	0.0155 (5)	−0.0731 (3)	0.7604 (3)	5.0 (1)	C(B2)	0.0124 (5)	0.3850 (3)	0.2442 (3)	4.9 (1)
C(A3)	0.0303 (6)	−0.0833 (4)	0.8281 (4)	6.4 (2)	C(B3)	0.0301 (6)	0.3426 (4)	0.1963 (4)	6.1 (2)
C(A4)	0.0628 (6)	−0.0353 (4)	0.8682 (4)	6.4 (2)	C(B4)	0.0867 (6)	0.2888 (4)	0.2115 (4)	6.0 (2)
C(A5)	0.0892 (7)	0.0212 (4)	0.8486 (4)	7.0 (2)	C(B5)	0.1246 (6)	0.2733 (3)	0.2741 (4)	5.9 (2)
C(A6)	0.0813 (6)	0.0326 (4)	0.7795 (4)	6.1 (2)	C(B6)	0.1085 (5)	0.3143 (3)	0.3225 (3)	4.9 (1)
C(A7)	−0.0257 (4)	−0.0733 (3)	0.6102 (3)	3.6 (1)	C(B7)	−0.0427 (4)	0.4905 (3)	0.3469 (3)	3.5 (1)
C(A8)	−0.1252 (5)	−0.0964 (3)	0.6148 (3)	4.6 (1)	C(B8)	−0.1278 (5)	0.5063 (3)	0.3744 (3)	4.0 (1)
C(A9)	−0.1619 (6)	−0.1526 (3)	0.5853 (4)	5.5 (1)	C(B9)	−0.1814 (5)	0.5637 (3)	0.3538 (3)	5.1 (1)
C(A10)	−0.0991 (6)	−0.1868 (4)	0.5512 (4)	6.0 (2)	C(B10)	−0.1500 (5)	0.6031 (3)	0.3122 (3)	5.3 (1)
C(A11)	−0.0020 (6)	−0.1645 (3)	0.5463 (3)	5.4 (1)	C(B11)	−0.0652 (5)	0.5887 (3)	0.2849 (3)	4.6 (1)
C(A12)	0.0370 (5)	−0.1073 (3)	0.5762 (3)	4.4 (1)	C(B12)	−0.0106 (5)	0.5329 (3)	0.3022 (3)	4.2 (1)
C(A13)	0.1434 (5)	0.0216 (3)	0.6303 (3)	3.8 (1)	C(B13)	−0.0153 (4)	0.3778 (3)	0.4313 (3)	3.6 (1)
C(A14)	0.1524 (5)	0.0725 (3)	0.5892 (3)	4.7 (1)	C(B14)	−0.1119 (5)	0.3486 (3)	0.4115 (3)	4.3 (1)
C(A15)	0.2455 (5)	0.0860 (3)	0.5704 (3)	5.4 (1)	C(B15)	−0.1567 (5)	0.3145 (3)	0.4558 (3)	5.1 (1)
C(A16)	0.3312 (6)	0.0479 (3)	0.5932 (4)	5.6 (1)	C(B16)	−0.1073 (5)	0.3085 (3)	0.5171 (3)	5.0 (1)
C(A17)	0.3241 (6)	−0.0019 (3)	0.6339 (4)	5.3 (1)	C(B17)	−0.0126 (6)	0.3348 (3)	0.5368 (3)	5.3 (1)
C(A18)	0.2308 (5)	−0.0154 (3)	0.6540 (3)	4.5 (1)	C(B18)	0.0369 (5)	0.3706 (3)	0.4937 (3)	4.1 (1)
C(A19)	−0.0768 (5)	0.0603 (3)	0.6269 (3)	4.1 (1)	C(B19)	0.1644 (4)	0.4572 (2)	0.4099 (3)	3.1 (1)
C(A20)	−0.0867 (6)	0.1123 (3)	0.6677 (3)	5.3 (1)	C(B20)	0.2582 (5)	0.4291 (3)	0.4055 (3)	4.2 (1)
C(A21)	−0.1620 (6)	0.1595 (4)	0.6478 (4)	6.1 (2)	C(B21)	0.3507 (5)	0.4594 (3)	0.4321 (3)	4.9 (1)
C(A22)	−0.2232 (6)	0.1543 (4)	0.5880 (4)	6.2 (2)	C(B22)	0.3508 (5)	0.5164 (3)	0.4619 (3)	4.4 (1)
C(A23)	−0.2142 (6)	0.1042 (4)	0.5473 (4)	6.2 (2)	C(B23)	0.2578 (5)	0.5446 (3)	0.4685 (3)	5.0 (1)
C(A24)	−0.1390 (5)	0.0559 (3)	0.5672 (3)	4.9 (1)	C(B24)	0.1647 (5)	0.5150 (3)	0.4425 (3)	4.2 (1)

[a] The isotropic thermal parameters are in units of Å^2. The anisotropic temperature factor has the form $T = -\Sigma(^1/_4 B_{ij} H_i H_j a_i^* a_j^*)$, where H is the Miller index, a^* is the reciprocal cell length, and i and j are cycled 1–3. The isotropic temperature factor has the form $T = -B[((\sin\theta)/\lambda)^2]$.

(B) $(Ph_4P)_2[(S_5)FeS_2MS_2]$ Complexes (M = Mo, W). The structures of the $[(S_5)FeS_2MS_2]^{2-}$ anions (Figure 2) show a central $S_2FeS_2MS_2$ unit very similar to the corresponding units in the $[(PhS)_2FeS_2MS_2]^{2-}$ complexes (Table V). The effects of charge delocalization in the MS_4^{2-} ligands again result in two short terminal Mo(W)–S bonds and two longer Mo(W)–S bridging bond lengths. The $\overline{M-S}$ bonds[35] in the coordinated MS_4^{2-} ligands (M = Mo, 2.204 Å; M = W, 2.208 Å) are slightly longer than the $\overline{M-S}$ bonds in the MS_4^{2-} anions (M = Mo, 2.176 (5) Å;[36] M = W, 2.17 (1) Å[37]) and nearly the same as the $\overline{M-S}$ bonds in the $[(PhS)_2FeS_2MS_2]^{2-}$ complexes. The $\overline{S-M-S}$ angles in the coordinated MS_4^{2-} anions (M = Mo, 109.38°; M = W, 109.43°) are very close to the ideal tetrahedral value.

The bond lengths within the FeS_4 tetrahedral units are similar to corresponding bond lengths in the $[(PhS)_2FeS_2MS_2]^{2-}$ complexes. In the $[(S_5)FeS_2MS_2]^{2-}$ anions the terminal Fe–S bond lengths (Fe–S_5 bonds) have a mean value of 2.33 (3) Å for M = Mo and 2.322 (11) Å for M = W. The bridging $\overline{Fe-S}$ bond length is 2.248 (4) Å for M = Mo and 2.269 (17) Å for M = W. The Fe–M distances are 2.737 (3) Å for M = Mo and 2.752 (3) Å for M = W. Collectively the slightly longer $\overline{Fe-S}$ terminal bonds and the slightly shorter $\overline{Fe-S}$ bridge bonds and Fe–M distances in the $[(S_5)FeS_2MS_2]^{2-}$ anions indicate somewhat stronger Fe–S_2MS_2 interactions when compared to those in the $[(PhS)_2FeS_2MS_2]^{2-}$ complexes. A similar conclusion can be reached from the values of the $(\overline{Fe-S}) - (\overline{Fe-S_b})$ and $(\overline{Fe-S}) - (\overline{Fe-S_t})$ differences. For M = Mo ($\overline{Fe-S}$ = 2.288 Å) these values are 0.04 (3) and −0.040 (4) Å, and for M = W ($\overline{Fe-S}$ = 2.295 Å) the corresponding values are 0.026 (17) and −0.026 (11) Å.

The FeS_4 units in the $[(S_5)FeS_2MS_2]^{2-}$ complexes are distorted from the ideal T_d symmetry, and the S–Fe–S angles range from 99.2 (2) to 118.0 (3)°. Unlike the FeS_4 units in the $[(PhS)_2FeS_2MS_2]^{2-}$ complexes, where specific intramolecular forces were identified as causes for the distortions, the FeS_4 units in the $[(S_5)FeS_2MS_2]^{2-}$ complexes are not subject to intramolecular crowding. In $Fe_2S_{12}^{2-}$, the only other Fe(III) complex that contains the $(S_5)FeS_2$ unit, the S–Fe–S angles are "normal" and span the range from 104.2 (2) to 114.8

Table III. Positional and Thermal Parameters and Their Standard Deviations in the Compound $[(C_2H_5)_4N]_2[(C_6H_5S)_2FeS_2WS_2]$[a]

atom	x	y	z	B_{11}	B_{22}	B_{33}	B_{12}	B_{13}	B_{23}
W	0.16616 (2)	0.19555 (3)	0.13455 (1)	2.62 (1)	2.65 (1)	3.14 (1)	−0.09 (1)	0.487 (8)	−0.02 (1)
Fe	0.34682 (9)	0.34413 (9)	0.10652 (3)	2.42 (4)	3.04 (5)	3.33 (4)	−0.03 (3)	0.61 (3)	−0.16 (3)
S(5)	0.1443 (2)	0.1839 (2)	0.20254 (6)	6.0 (1)	5.1 (1)	3.59 (9)	−0.9 (1)	1.26 (8)	0.14 (8)
S(2)	0.4521 (2)	0.4814 (2)	0.15515 (7)	2.71 (7)	4.7 (1)	4.6 (1)	0.14 (7)	0.56 (7)	−1.72 (8)
S(4)	0.1467 (2)	0.3927 (2)	0.11214 (7)	2.72 (7)	2.86 (8)	5.3 (1)	0.33 (6)	0.89 (7)	0.13 (7)
S(1)	0.4083 (2)	0.3864 (2)	0.03989 (6)	3.26 (8)	4.03 (9)	3.47 (8)	−0.69 (7)	0.76 (6)	−0.13 (7)
S(6)	0.0313 (2)	0.0817 (2)	0.09623 (7)	3.87 (9)	4.0 (1)	5.2 (1)	−0.80 (8)	−0.80 (8)	−0.94 (8)
S(3)	0.3573 (2)	0.1376 (2)	0.12396 (7)	3.07 (8)	3.36 (9)	5.0 (1)	0.87 (7)	0.49 (7)	0.16 (8)
N(1)	0.7267 (6)	0.2780 (6)	0.4705 (2)	3.3 (3)	4.0 (4)	5.6 (4)	−1.3 (3)	0.0 (3)	1.0 (3)
N(2)	0.7318 (5)	0.0217 (6)	0.2216 (2)	3.6 (3)	5.0 (4)	2.8 (3)	−0.2 (3)	1.0 (2)	0.9 (2)
C(11)	0.3082 (6)	0.3235 (6)	−0.0040 (2)	2.6 (3)	3.1 (3)	3.1 (3)	0.6 (2)	0.8 (2)	−0.5 (3)
C(16)	0.3064 (7)	0.3770 (7)	−0.0442 (2)	4.9 (4)	3.0 (4)	3.7 (4)	−0.2 (3)	0.8 (3)	0.2 (3)
C(15)	0.2322 (9)	0.3300 (9)	−0.0798 (3)	5.9 (5)	5.6 (5)	3.9 (4)	−0.2 (4)	−0.1 (3)	0.8 (3)
C(14)	0.1581 (8)	0.2277 (9)	−0.0755 (3)	5.2 (5)	6.4 (6)	4.0 (4)	0.2 (4)	−1.2 (3)	−0.9 (4)
C(13)	0.1591 (7)	0.1765 (8)	−0.0354 (3)	4.4 (4)	4.2 (4)	4.9 (4)	−1.5 (3)	−0.2 (3)	−0.6 (3)
C(12)	0.2328 (7)	0.2224 (7)	0.0006 (2)	3.4 (3)	3.7 (4)	4.0 (3)	−0.1 (3)	0.4 (3)	−0.1 (3)
C(21)	0.6110 (6)	0.4526 (7)	0.1612 (2)	3.1 (3)	3.2 (3)	3.7 (3)	−0.2 (3)	0.4 (3)	−0.1 (3)
C(22)	0.6684 (6)	0.3836 (7)	0.1325 (2)	2.8 (3)	4.0 (4)	3.7 (3)	0.4 (3)	0.3 (2)	−0.2 (3)
C(23)	0.7934 (7)	0.3634 (9)	0.1287 (3)	3.5 (3)	5.7 (5)	4.2 (4)	0.7 (3)	0.8 (3)	−0.7 (3)
C(24)	0.8645 (7)	0.4135 (9)	0.1736 (3)	2.7 (3)	6.7 (5)	5.7 (5)	0.9 (3)	0.6 (3)	−1.1 (4)
C(25)	0.8084 (8)	0.482 (1)	0.2029 (3)	3.7 (4)	8.5 (7)	6.4 (5)	0.3 (4)	−0.9 (4)	−3.8 (5)
C(26)	0.6833 (7)	0.5019 (9)	0.1969 (3)	3.4 (4)	7.5 (6)	5.1 (5)	0.6 (4)	0.2 (3)	−3.5 (4)
C(30)	0.7485 (9)	0.3747 (9)	0.5050 (3)	6.5 (5)	5.1 (5)	5.7 (5)	−1.4 (4)	0.6 (4)	0.8 (4)
C(31)	0.687 (1)	0.350 (1)	0.5460 (4)	7.9 (8)	10.2 (8)	6.4 (6)	−0.9 (6)	1.4 (5)	1.9 (5)
C(32)	0.7913 (9)	0.3246 (9)	0.4334 (3)	5.5 (5)	4.9 (5)	6.9 (5)	−1.8 (4)	1.5 (4)	−0.4 (4)
C(33)	0.779 (1)	0.245 (1)	0.3931 (4)	12.1 (10)	7.8 (8)	9.2 (8)	−2.4 (7)	4.2 (7)	−2.8 (7)
C(34)	0.776 (1)	0.1538 (9)	0.4886 (4)	7.4 (6)	3.7 (5)	11.1 (8)	−1.1 (4)	0.3 (6)	2.1 (5)
C(35)	0.909 (1)	0.152 (1)	0.5056 (5)	6.7 (6)	5.7 (6)	16.1 (12)	0.6 (5)	−1.1 (7)	2.7 (7)
C(36)	0.5914 (9)	0.257 (1)	0.4543 (3)	5.2 (5)	6.2 (5)	6.4 (5)	−2.3 (4)	0.2 (4)	1.4 (4)
C(37)	0.5204 (9)	0.376 (1)	0.4410 (4)	4.9 (5)	8.2 (7)	8.0 (7)	−0.8 (5)	−0.5 (4)	3.2 (6)
C(38)	0.7890 (7)	0.0355 (9)	0.2680 (3)	4.3 (4)	5.7 (5)	3.8 (4)	0.2 (4)	1.2 (3)	0.6 (3)
C(39)	0.8678 (9)	0.147 (1)	0.2785 (3)	6.4 (5)	7.2 (6)	5.6 (5)	−0.3 (5)	1.4 (4)	−1.3 (4)
C(40)	0.6547 (8)	0.1343 (9)	0.2058 (3)	5.2 (4)	5.2 (5)	4.3 (4)	1.3 (4)	1.3 (3)	1.5 (3)
C(41)	0.5521 (9)	0.164 (1)	0.2322 (3)	6.4 (5)	7.5 (7)	6.4 (5)	2.7 (5)	2.5 (4)	2.3 (5)
C(42)	0.8290 (7)	0.0112 (9)	0.1912 (3)	4.8 (4)	5.6 (5)	3.4 (4)	0.2 (4)	1.2 (3)	1.1 (3)
C(43)	0.9151 (8)	−0.0982 (9)	0.1994 (3)	4.4 (4)	6.0 (5)	6.1 (5)	0.8 (4)	1.5 (4)	−0.0 (4)
C(44)	0.6536 (8)	−0.0938 (9)	0.2207 (3)	4.3 (4)	6.1 (5)	5.8 (5)	−0.9 (4)	0.5 (3)	2.8 (4)
C(45)	0.5889 (9)	−0.132 (1)	0.1760 (4)	6.2 (5)	6.6 (6)	7.1 (6)	−1.3 (5)	−1.3 (5)	1.0 (5)

[a] The anisotropic temperature factor has the form $T = -\Sigma(^1/_4 B_{ij} H_i H_j a_i^* a_j^*)$, where H is the Miller index, a^* is the reciprocal cell length, and i and j are cycled 1–3.

(2)°.[28] The pronounced distortions of the FeS_4 units in the $[(S_5)FeS_2MS_2]^{2-}$ complexes must therefore arise because of crystal packing forces. An examination of intermolecular contacts shows that two of the sulfur atoms (S(3), S(4) are near the cation hydrogen atoms (H(32), H(91), H(97)) at distances greater than 2.7 Å and less than 3.00 Å. The layered anion–cation packing in the crystal is shown in Figure 3.

The S_5^{2-} anion, although not a common ligand, occurs as a bidentate chelate in the $[PtS_{15}]^{2-}$,[40] $Ti(Cp)_2S_5$,[41] and $Fe_2S_{12}^{2-}$[28] complexes. Structure determinations of the $[PtS_{15}]^{2-}$[42] and $Fe_2S_{12}^{2-}$[28] complexes show the PtS_5 and FeS_5 "rings" in the chair conformation not unlike the conformation found in the present structures. Structural details of the chelated S_5^{2-} ligands in the $[(S_5)FeS_2MS_2]^{2-}$ complexes (Table V) are similar to those found in the $[PtS_{15}]^{2-}$ and $Fe_2S_{12}^{2-}$ complexes and will not be discussed any further. Partial occupation of the same site by either S_5^{2-} or S_6^{2-} in the $[(S_5)FeS_2MoS_2]^{2-}$ anion, and the close proximity of S(9), S(9)′, and S(10) to each other, result in a loss of both precision and accuracy in the dimensions of the coordinated S_5^{2-} and S_6^{2-} chelates. To our knowledge, previous examples of a coordinated S_6^{2-} ligand are not available.[30]

The FeS_2M Dimetallic Unit. A feature common to all of the $L_2FeS_2MS_2$ complexes is the rhombic FeS_2M unit. The dimensions of this unit are quite similar for all of the complexes, and the magnitudes of the Fe–M distances and the Fe–S–M angles are found in relatively narrow ranges. For the complexes reported herein the $\overline{\text{Fe–Mo}}$ distance, $\overline{S_b–S_b}$ distance, and $\overline{\text{Fe–S–Mo}}$ angle are 2.74 (1) Å, 3.59 (1) Å, and 74.6 (2)°, respectively. In the W analogues the $\overline{\text{Fe–W}}$ dis-

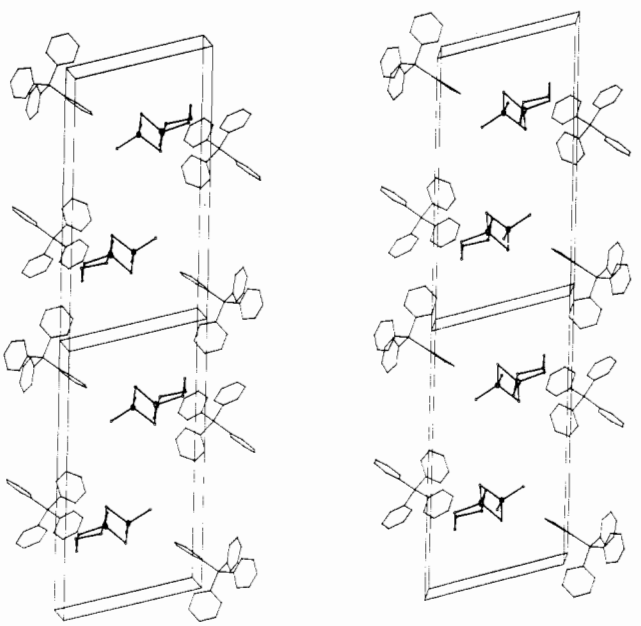

Figure 3. Packing diagram (two unit cells) for $[(C_6H_5)_4P]_2[(S_5)FeS_2MS_2]$ (M = Mo, W). The DMF molecules of solvation and the S_6 minor component have been omitted for clarity.

(40) Hofmann, K. A.; Höchtlen, F. *Chem. Ber.* **1903**, *36*, 3090.
(41) Köpf, H.; Block, B.; Schmidt, M. *Chem. Ber.* **1968**, *101* 272.
(42) Jones, P. E.; Katz, L. *Acta Crystallogr., Sect. B.* **1969**, *B25*, 745.

Table IV. Positional and Thermal Parameters and Their Standard Deviations in the Compound $[(C_6H_5)_4P]_2[(S_5FeS_2MoS_2)_{0.70}(S_6FeS_2MoS_2)_{0.30}]$[a]

atom	x	y	z	B or B_{11}	B_{22}	B_{33}	B_{12}	B_{13}	B_{23}
Fe	0.6378 (2)	0.2694 (1)	−0.0662 (3)	3.8 (1)	4.9 (1)	4.3 (1)	1.5 (1)	−0.3 (1)	0.5 (1)
Mo	0.4843 (1)	0.26925 (8)	0.1576 (2)	2.68 (7)	3.77 (8)	5.42 (9)	0.75 (6)	0.59 (6)	1.52 (6)
S(1)	0.8282 (4)	0.2583 (3)	−0.0885 (5)	4.0 (2)	6.2 (3)	3.7 (2)	1.8 (2)	−0.0 (2)	0.6 (2)
S(3)	0.4878 (5)	0.1872 (2)	−0.0258 (7)	4.7 (2)	3.3 (2)	10.8 (4)	0.3 (2)	−1.7 (3)	−0.2 (2)
S(4)	0.6441 (4)	0.3484 (2)	0.1215 (5)	3.4 (2)	3.8 (2)	4.5 (2)	0.1 (2)	−0.3 (2)	0.0 (2)
S(5)	0.5093 (6)	0.2449 (4)	0.3298 (7)	7.2 (3)	10.9 (5)	6.4 (3)	3.4 (3)	1.0 (3)	4.2 (3)
S(6)	0.3288 (5)	0.3029 (3)	0.1841 (8)	5.0 (3)	6.2 (3)	10.6 (5)	2.3 (3)	0.6 (3)	1.7 (3)
S(7)	0.8290 (6)	0.1889 (3)	−0.2615 (6)	8.7 (4)	5.6 (3)	4.9 (3)	3.1 (3)	−1.0 (3)	−0.2 (2)
S(2)	0.6128 (7)	0.3085 (3)	−0.2373 (7)	7.9 (2)					
S(8)	0.8250 (6)	0.2297 (3)	−0.4027 (6)	7.1 (1)					
S(9)	0.643 (1)	0.2274 (5)	−0.387 (1)	6.5 (2)					
S(9′)	0.698 (3)	0.222 (1)	−0.465 (3)	9.5 (7)					
S(10)	0.574 (5)	0.225 (2)	−0.340 (4)	14.1 (12)					
P(1)	0.8290 (4)	0.0132 (2)	0.2926 (4)	4.4 (2)	4.1 (2)	3.6 (2)	1.1 (2)	−0.7 (2)	1.0 (2)
P(2)	−0.1045 (4)	0.5875 (2)	0.4092 (4)	3.6 (2)	3.3 (2)	2.9 (2)	0.5 (2)	−0.6 (2)	0.2 (2)
C(1)	−0.241 (2)	0.0344 (8)	0.183 (2)	4.0 (8)	3.5 (9)	4.3 (9)	1.0 (7)	0.5 (7)	2.4 (7)
C(2)	−0.252 (2)	0.0967 (9)	0.217 (2)	8.2 (13)	3.4 (9)	5.0 (11)	1.3 (9)	−1.6 (10)	0.9 (8)
C(3)	−0.312 (2)	0.116 (1)	0.140 (2)	4.8 (10)	4.4 (10)	6.7 (13)	0.6 (9)	−0.1 (10)	2.8 (10)
C(4)	−0.349 (2)	0.071 (1)	0.026 (3)	2.6 (8)	5.6 (13)	11.8 (20)	1.1 (9)	−1.4 (10)	3.0 (13)
C(5)	−0.331 (3)	0.016 (1)	−0.013 (3)	9.5 (17)	5.5 (13)	7.9 (15)	1.0 (12)	−4.0 (14)	1.7 (12)
C(6)	−0.275 (2)	−0.0078 (8)	0.061 (2)	4.7 (9)	3.6 (8)	3.7 (9)	0.4 (7)	−1.7 (8)	−0.7 (7)
C(7)	−0.043 (1)	0.0759 (9)	0.340 (2)	2.7 (7)	6.1 (10)	3.9 (9)	1.4 (8)	−0.7 (7)	1.5 (9)
C(8)	0.033 (2)	0.1042 (9)	0.252 (2)	5.0 (11)	4.5 (10)	6.3 (13)	0.0 (10)	−1.8 (10)	1.6 (10)
C(9)	0.136 (2)	0.1492 (9)	0.273 (2)	7.8 (15)	3.7 (10)	6.9 (14)	0.4 (11)	2.2 (12)	1.9 (10)
C(10)	0.161 (2)	0.168 (1)	0.406 (2)	6.2 (12)	5.3 (11)	4.9 (12)	−2.3 (10)	−2.0 (10)	−0.4 (9)
C(11)	0.089 (2)	0.145 (1)	0.504 (3)	4.4 (11)	8.0 (14)	7.8 (15)	2.1 (11)	−3.2 (11)	−1.4 (13)
C(12)	−0.014 (2)	0.0940 (9)	0.466 (2)	4.2 (10)	4.8 (10)	6.0 (12)	1.1 (9)	−0.3 (9)	0.9 (9)
C(13)	−0.123 (2)	−0.0594 (9)	0.201 (2)	5.8 (11)	4.5 (9)	1.7 (7)	1.9 (9)	−0.2 (7)	0.5 (7)
C(14)	−0.202 (2)	−0.117 (1)	0.158 (2)	5.8 (11)	4.2 (10)	7.8 (13)	−0.8 (10)	−5.0 (11)	1.7 (10)
C(15)	−0.163 (4)	−0.169 (1)	0.088 (3)	18.5 (33)	2.2 (11)	6.6 (15)	2.5 (16)	−2.6 (18)	1.1 (10)
C(16)	−0.052 (3)	−0.170 (1)	0.066 (2)	8.3 (15)	7.0 (16)	5.3 (12)	4.5 (15)	0.0 (12)	1.3 (11)
C(17)	0.030 (2)	−0.111 (1)	0.117 (2)	6.8 (12)	6.9 (13)	5.4 (11)	5.5 (13)	3.0 (10)	1.9 (10)
C(18)	−0.005 (2)	−0.057 (1)	0.186 (2)	4.3 (10)	6.0 (11)	2.1 (7)	1.7 (9)	1.0 (7)	0.4 (8)
C(19)	−0.273 (2)	0.0009 (9)	0.434 (2)	5.9 (10)	2.4 (8)	3.4 (9)	1.5 (8)	0.4 (8)	−0.6 (7)
C(20)	−0.297 (3)	−0.055 (2)	0.472 (3)	9.2 (17)	10.5 (19)	7.8 (17)	7.0 (6)	0.2 (14)	1.7 (15)
C(21)	−0.379 (3)	−0.060 (2)	0.582 (3)	11.2 (21)	11.0 (20)	6.0 (15)	0.9 (17)	4.6 (15)	6.0 (16)
C(22)	−0.424 (2)	−0.015 (2)	0.657 (2)	7.7 (15)	10.2 (19)	4.5 (13)	1.7 (15)	1.1 (11)	1.8 (14)
C(23)	−0.401 (2)	0.042 (1)	0.623 (2)	7.1 (12)	6.2 (12)	2.9 (9)	−0.8 (10)	−1.4 (9)	1.3 (9)
C(24)	−0.320 (2)	0.048 (1)	0.510 (2)	9.4 (16)	5.3 (12)	5.4 (13)	−1.4 (12)	−1.8 (12)	1.6 (11)
C(25)	−0.022 (1)	0.5413 (7)	0.272 (1)	2.6 (7)	2.5 (7)	2.6 (7)	1.1 (6)	1.2 (6)	1.1 (6)
C(26)	0.080 (2)	0.5772 (8)	0.221 (2)	5.7 (11)	4.4 (9)	3.0 (8)	2.3 (9)	−0.1 (8)	2.2 (8)
C(27)	0.146 (2)	0.5402 (9)	0.113 (2)	6.0 (11)	3.9 (9)	5.4 (11)	1.2 (9)	−1.1 (9)	1.0 (9)
C(28)	0.108 (2)	0.476 (1)	0.067 (2)	7.5 (15)	7.4 (14)	3.9 (10)	4.1 (13)	0.0 (10)	−0.2 (10)
C(29)	0.002 (2)	0.4441 (8)	0.122 (2)	3.2 (8)	2.8 (8)	5.4 (10)	1.7 (7)	1.7 (8)	0.4 (8)
C(30)	−0.061 (2)	0.4780 (9)	0.227 (2)	4.6 (9)	3.6 (9)	4.3 (10)	0.9 (8)	−0.7 (8)	1.2 (8)
C(31)	−0.219 (1)	0.5343 (7)	0.481 (1)	3.5 (7)	2.0 (6)	1.1 (6)	−0.3 (6)	−1.5 (6)	−0.6 (5)
C(32)	−0.315 (2)	0.4957 (8)	0.411 (2)	4.5 (9)	3.3 (8)	2.9 (8)	0.5 (8)	−1.0 (7)	1.0 (7)
C(33)	−0.401 (2)	0.4495 (9)	0.461 (2)	3.6 (8)	4.0 (9)	3.4 (9)	0.9 (8)	−1.4 (7)	−1.0 (7)
C(34)	−0.396 (2)	0.4451 (9)	0.584 (3)	3.6 (9)	3.3 (9)	10.0 (18)	0.1 (8)	−1.1 (11)	1.9 (10)
C(35)	−0.308 (2)	0.482 (1)	0.659 (2)	5.0 (11)	6.6 (12)	5.7 (12)	2.2 (11)	1.5 (10)	3.1 (10)
C(36)	−0.219 (1)	0.5247 (8)	0.606 (2)	2.7 (8)	4.9 (9)	3.6 (9)	−1.0 (8)	−0.7 (7)	1.0 (8)
C(37)	−0.173 (1)	0.6352 (7)	0.352 (2)	2.2 (7)	2.7 (7)	4.6 (9)	0.1 (6)	−0.5 (7)	0.9 (7)
C(38)	−0.118 (1)	0.6557 (8)	0.237 (2)	3.4 (7)	4.0 (8)	4.1 (9)	1.3 (7)	0.1 (7)	2.1 (7)
C(39)	−0.174 (2)	0.689 (1)	0.192 (2)	10.0 (17)	5.4 (11)	5.8 (12)	3.9 (12)	0.7 (11)	4.1 (10)
C(40)	−0.281 (2)	0.7030 (8)	0.257 (2)	4.6 (9)	3.1 (8)	9.6 (16)	1.5 (8)	−3.3 (10)	1.8 (10)
C(41)	−0.328 (1)	0.6837 (8)	0.369 (2)	3.4 (8)	3.5 (8)	4.5 (10)	−0.0 (7)	0.8 (7)	2.0 (8)
C(42)	−0.274 (2)	0.6494 (8)	0.416 (2)	5.5 (11)	2.4 (7)	3.7 (9)	0.7 (7)	−1.3 (8)	0.4 (6)
C(43)	−0.006 (1)	0.6354 (8)	0.530 (2)	3.3 (8)	3.4 (8)	2.1 (7)	−0.1 (7)	1.1 (6)	1.0 (7)
C(44)	−0.039 (1)	0.690 (1)	0.617 (2)	1.8 (6)	6.2 (11)	4.3 (9)	1.4 (7)	0.8 (7)	0.5 (9)
C(45)	0.039 (2)	0.7274 (9)	0.720 (2)	7.6 (13)	4.4 (10)	1.8 (8)	1.6 (10)	−1.0 (8)	−2.2 (7)
C(46)	0.135 (2)	0.712 (1)	0.728 (2)	5.5 (12)	5.0 (12)	6.5 (13)	−1.3 (10)	−2.2 (10)	2.7 (11)
C(47)	0.166 (2)	0.660 (1)	0.637 (2)	5.3 (10)	3.6 (10)	9.1 (15)	−0.2 (9)	−3.9 (11)	1.9 (11)
C(48)	0.094 (1)	0.6220 (7)	0.539 (2)	3.8 (8)	2.5 (7)	3.7 (8)	1.1 (7)	−1.6 (7)	0.2 (6)
N	0.500	0.500	0	7.0 (6)					
C(51)	0.473 (4)	0.447 (2)	0.041 (5)	6.1 (10)					
C(49)	0.438 (4)	0.514 (2)	−0.080 (4)	5.9 (9)					
C(50)	0.575 (6)	0.550 (3)	0.045 (7)	9.1 (14)					
O	0.647 (3)	0.527 (2)	0.149 (3)	7.6 (8)					

[a] The anisotropic temperature factor has the form $T = -\Sigma(^1/_4 B_{ij} H_i H_j a^*_i a^*_j)$, where H is the Miller index, a^* is the reciprocal cell length, and i and j are cycled 1-3. The isotropic temperature factor has the form $T = -B[((\sin\theta)/\lambda)^2]$, with B in Å^2.

tance, $\overline{S_b–S_b}$ distance, and $\overline{Fe–S–W}$ angle are 2.76 (2) Å, 3.588 (7) Å, and 75.2 (5)°, respectively. Depending on the nature of Fe–M interactions (bonding vs. nonbonding), the Fe–M distances may be the cause or a consequence of relative bridge strengths. A consideration of the rather short Fe–M distances strongly suggests that there must be appreciable overlap between the metal d_{z^2} orbitals in a coordinate scheme where the z axis passes through the metal atoms. However

Table V. Intramolecular Bond Distances (Å) and Angles (deg) in the $[L_2FeS_2MS_2]^{2-}$ Anions[a]

	$[(C_6H_5)_4P]_2$-$[(C_6H_5S)_2FeS_2MoS_2]$	$[(C_2H_5)_4N]_2$-$[(C_6H_5S)_2FeS_2WS_2]$	$[(C_6H_5)_4P]_2$-$[(S_5)FeS_2MoS_2]$[b]	$[(C_6H_5)_4P]_2$-$[(S_5)FeS_2WS_2]$[b]
		Distances		
Mo(W)-Fe	2.740 (1)	2.775 (1)	2.737 (3)	2.752 (3)
Mo(W)-S(3)	2.255 (2)	2.254 (2)	2.262 (5)	2.273 (7)
Mo(W)-S(4)	2.269 (2)	2.239 (2)	2.259 (4)	2.246 (6)
Mo(W)-S(5)	2.153 (2)	2.154 (2)	2.161 (6)	2.168 (8)
Mo(W)-S(6)	2.145 (2)	2.159 (2)	2.135 (6)	2.145 (6)
Fe-S(1)	2.292 (2)	2.298 (2)	2.308 (5)	2.314 (6)
Fe-S(2)	2.303 (2)	2.314 (2)	2.349 (8)	2.330 (8)
Fe-S(3)	2.260 (2)	2.292 (2)	2.251 (6)	2.281 (7)
Fe-S(4)	2.265 (2)	2.288 (2)	2.246 (5)	2.257 (7)
S(1)-C(11)	1.804 (7)	1.770 (7)		
S(2)-C(21)	1.747 (8)	1.758 (7)		
C(11)-C(12)	1.380 (10)	1.388 (10)		
C(12)-C(13)	1.367 (11)	1.382 (10)		
C(13)-C(14)	1.381 (12)	1.360 (12)		
C(14)-C(15)	1.378 (12)	1.388 (12)		
C(15)-C(16)	1.370 (11)	1.381 (11)		
C(16)-C(11)	1.374 (10)	1.371 (10)		
C(21)-C(22)	1.398 (10)	1.373 (10)		
C(22)-C(23)	1.413 (11)	1.379 (10)		
C(23)-C(24)	1.368 (15)	1.364 (11)		
C(24)-C(25)	1.360 (16)	1.375 (12)		
C(25)-C(26)	1.399 (15)	1.380 (11)		
C(26)-C(21)	1.388 (11)	1.381 (10)		
S(1)-S(7)			2.036 (7)	2.032 (9)
S(7)-S(8)			2.001 (9)	2.036 (10)
S(8)-S(9)			2.123 (12)	2.060 (13)
S(9)-S(2)			2.113 (13)	2.079 (12)
S(1)-S(2)	3.866 (3)	3.687 (3)	3.814 (9)	3.867 (10)
S(1)-S(3)	3.781 (3)	3.831 (3)	3.907 (7)	3.930 (8)
S(1)-S(4)	3.631 (3)	3.862 (3)	3.467 (6)	3.483 (8)
S(2)-S(3)	3.513 (3)	3.939 (3)	3.858 (10)	3.832 (12)
S(2)-S(4)	3.915 (3)	3.578 (3)	3.734 (9)	3.722 (10)
S(3)-S(4)	3.600 (2)	3.583 (3)	3.580 (6)	3.593 (9)
S(3)-S(5)	3.625 (3)	3.620 (3)	3.666 (10)	3.615 (11)
S(3)-S(6)	3.552 (3)	3.624 (3)	3.638 (8)	3.636 (9)
S(4)-S(5)	3.630 (3)	3.596 (3)	3.548 (8)	3.614 (10)
S(4)-S(6)	3.622 (3)	3.598 (3)	3.578 (8)	3.588 (8)
S(5)-S(6)	3.566 (3)	3.544 (3)	3.571 (9)	3.578 (10)
S(8)-S(9′)			1.70 (3)	
S(9′)-S(10)			1.81 (5)	
S(10)-S(2)			1.84 (5)	
S(9)-S(10)			0.88 (4)	
S(9)-S(9′)			0.96 (3)	
		Angles		
Mo(W)-S(3)-Fe	74.72 (5)	75.24 (5)	74.7 (2)	74.4 (2)
Mo(W)-S(4)-Fe	74.34 (5)	75.61 (5)	74.8 (2)	75.4 (2)
S(3)-Mo(W)-S(4)	105.50 (9)	105.80 (9)	104.7 (3)	105.3 (3)
S(3)-Mo(W)-S(5)	110.65 (11)	110.40 (11)	111.9 (3)	109.0 (4)
S(3)-Mo(W)-S(6)	107.67 (10)	110.39 (11)	111.6 (3)	110.7 (4)
S(4)-Mo(W)-S(5)	110.35 (10)	109.89 (11)	106.7 (3)	109.9 (3)
S(4)-Mo(W)-S(6)	110.28 (9)	109.76 (10)	109.0 (3)	109.6 (4)
S(5)-Mo(W)-S(6)	112.15 (11)	110.50 (11)	112.4 (3)	112.1 (3)
S(1)-Fe-S(2)	114.57 (9)[d]	106.15 (10)[e]	110.0 (3)	112.8 (3)
S(1)-Fe-S(3)	112.33 (10)[d]	113.14 (10)[d]	118.0 (3)	117.6 (4)
S(1)-Fe-S(4)	105.65 (9)[e]	114.74 (10)[d]	99.2 (2)	99.3 (3)
S(2)-Fe-S(3)	100.67 (10)[e]	117.56 (10)[d]	114.0 (3)	112.4 (4)
S(2)-Fe-S(4)	117.91 (9)[c]	102.06 (9)[e]	108.7 (3)	108.5 (4)
S(3)-Fe-S(4)	105.42 (9)	102.96 (9)	105.5 (3)	104.7 (3)
Fe-S(1)-C(11)	109.0 (2)	112.9 (2)		
Fe-S(2)-C(21)	112.2 (3)[d]	111.3 (3)[d]		
S(1)-C(11)-C(12)	124.2 (4)[d]	122.9 (4)[d]		
S(1)-C(11)-C(16)	118.3 (4)	118.2 (4)		
S(2)-C(21)-C(22)	122.7 (4)[d]	123.9 (4)[d]		
S(2)-C(21)-C(26)	119.3 (5)[e]	118.6 (4)[e]		
C(12)-C(11)-C(16)	117.4 (7)[e]	119.0 (7)[e]		
C(22)-C(21)-C(26)	117.8 (7)	117.5 (7)		
Fe-S(2)-S(9)			94.3 (3)	95.0 (4)
Fe-S(1)-S(7)			100.8 (2)	100.0 (3)
S(1)-S(7)-S(8)			106.4 (4)	107.7 (5)
S(8)-S(9)-S(2)			108.0 (5)	108.2 (5)

[a] The structural parameters for the counterions in the complexes are unexceptional. Thus, for $(C_6H_5)_4P^+$ in $(Ph_4P)_2[(PhS)_2FeS_2MoS_2]$ the mean value for the P-C bonds is 1.800 (11) Å (range 1.790 (6)-1.812 (6) Å) and the mean value for the C-C bonds in the phenyl rings is 1.38 (7) Å (range 1.317 (11)-1.456 (11) Å). In $(Et_4N)_2[(PhS)_2FeS_2WS_2]$ the C-N bond in the $(C_2H_5)_4N^+$ cations is 1.512 (11) Å (range

Table V (*Continued*)

1.492 (12)–1.524 (12) Å and the C–C bond is 1.51 (2) Å (range 1.492 (14)–1.536 (15) Å). For the $(C_6H_5)_4P^+$ cations in $(Ph_4P)_2[(S_5)FeS_2WS_2]\cdot{}^1/_2DMF$ the P–C bond is 1.79 (2) Å (range 1.76 (2)–1.82 (2) Å) and the C–C bond in the phenyl rings is 1.37 (3) Å (range 1.30 (3)–1.44 (4) Å). The corresponding data in the Mo analogue are 1.80 (2) Å (range 1.76 (2)–1.84 (2) Å) and 1.37 (4) Å (range 1.25 (3)–1.46 (3) Å). In all cases the standard deviations from the mean have been obtained as follows: $\sigma = [\Sigma_{i=1}^{N}(x - \bar{x})^2/N - 1]^{1/2}$, where x_i is the length of the bond and $\bar{x}$ is the mean value for the N equivalent bond lengths. [b] Crystallizes with one molecule of DMF in the unit cell (see also Tables I and IV). [c] The italicized angles deviate from expected values because of systematic intramolecular distortions as described in the text. [d] Values larger than those normally expected and consistent with ortho-hydrogen–S atom repulsions. [e] Values smaller than those normally expected and consistent with ortho-hydrogen–S atom repulsions (see also ref 14).

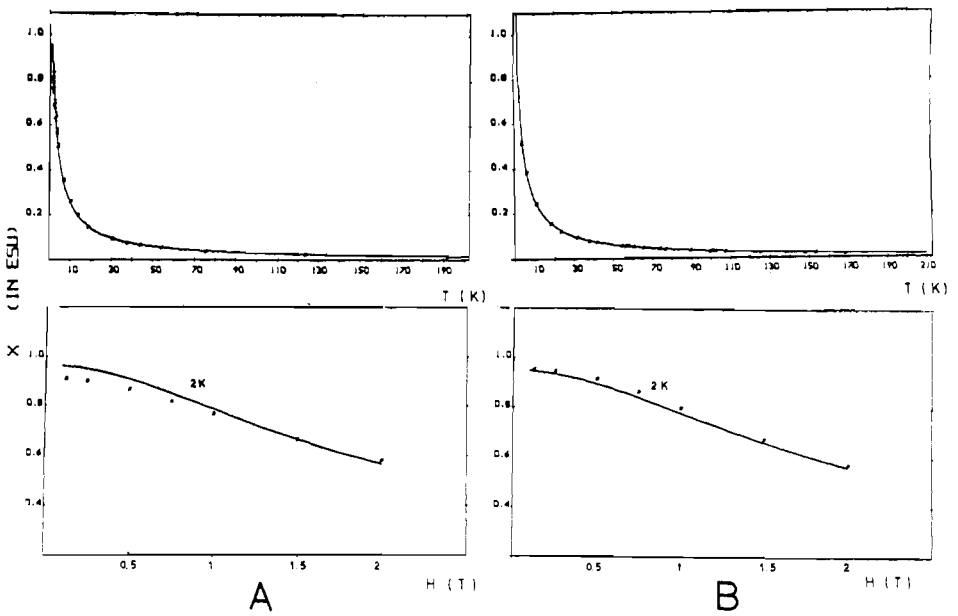

Figure 4. Temperature variation and field dependence of the inverse magnetic susceptibility of the $[(PhS)_2FeS_2MS_2]^{2-}$ complexes. The solid lines represent least-squares fits of the experimental data for M = Mo (A) and M = W (B).

any Fe(II)–M(VI) bonding interactions will depend on the relative energy matching of the d_{z^2} functions in the two metal ions. It has been emphasized[7] that the short Fe–M distances in the $Fe–MS_4$ complexes are not *necessarily* the result of M–M interactions. They can be accounted for, at least partially, as a result of structural constraints imposed by the acute Fe–S–M angles.

In other $M–MS_4$ complexes that contain the $M'S_2M$ rhombic unit (M' = Ni(II),[43] Co(II),[44] Zn(II)[32]) the M'–M distances and M'–S–M angles are similar to those found in the $Fe–MS_4$ complexes.[7] The short Zn–W distance in the $[(S_2WS_2)_2Zn]^{2-}$ complex at 2.927 (1) Å[32] is particularly interesting. In this complex extensive Zn → W charge transfer (and metal–metal bonding) is not likely to occur and the short Zn–W distance must be a consequence of the acute Zn–S–W angle of 78.5 (2)°.

An interesting characteristic of the rhombic FeS_2M unit in most of the $Fe–S_2MS_2$ complexes is a slight "folding" about the S–S vector. The FeS_2/S_2M dihedral angles in the $[Et_4N]_2[(PhS)_2FeS_2MS_2]$ complexes are 7.05 and 7.68°, respectively, for M = Mo and W. The corresponding dihedral angles in the $(Ph_4P)_2[(S_5)FeS_2MS_2]$ complexes are 8.33 and 5.42° for the Mo and W homologues. The same dihedral angle in the $[Fe(S_2MoS_2)_2]^{3-}$ complex[45] is 9.08°. The persistent occurrence of this folding may be rationalized in terms of direct (weak) M–Fe bonding, rather than crystal forces. The absence of any significant "folding" of the FeS_2Mo core in $(Ph_4P)_2[(PhS)_2FeS_2MoS_2]$ (1.2°) probably is a result of crystal forces. A certain flexibility of the FeS_2Mo core also is apparent when the intracore distances and angles are compared in the structures of the Et_4N^+ and Ph_4P^+ salts of the $[(PhS)_2FeS_2MoS_2]^{2-}$ anions. Thus, significantly shorter Fe–Mo distances, smaller Fe–S–Mo angles, and larger S_b–Fe–S_b angles are observed in the structure of the Ph_4P^+ salt by comparison to the Et_4N^+ salt. It seems as if the FeS_2Mo rhombic unit has a limited freedom to expand or contract along the Fe–Mo axis without an appreciable change in the Fe–S_b or Mo–S_b distances. This apparent flexibility in the $Fe–S_2–M$ cores allows for an adjustment of the Fe–M distances in the presence of crystal constraints.

Results of Mössbauer and Magnetic Susceptibility Measurements. (a) $(Ph_4P)_2[(PhS)_2FeS_2MS_2]$ (M = Mo, W). The magnetic susceptibility measurements for the Mo complex as a function of temperature and external magnetic field are shown in Figure 4. The solid lines represent fits of the data according to the electronic spin Hamiltonian

$$H_e = D(S_z^2 - 2) + E(S_x^2 - S_y^2) + \vec{S}\cdot g\cdot\vec{H}_{ext} \qquad (1)$$

where D and E are the axial and rhombic zero-field splitting parameters, respectively, and the last term represents the Zeeman interaction due to an external magnetic field, H_{ext}. The Hamiltonian has been written for an $S = 2$ spin system since the saturation magnetic moment ($\mu_{eff} = 4.90\ \mu_B$) suggests a divalent state for the iron ion. The parameters D and E determined in this way[46] have been deposited in the supplementary material. Similar are the data and analysis for the W homologue. The magnetic ordering that occurs at 4.2 K

(43) Søtofte, I. *Acta Chim. Scand., Ser. A.* **1976**, *A30*, 157.
(44) Müller, A.; Mohan, N.; Bögge, H. *Z. Naturforsch, B: Anorg. Chem., Org. Chem.* **1978**, *33B*, 978.
(45) Coucouvanis, D.; Simhon, E. D.; Baenziger, N. C. *J. Am. Chem. Soc.* **1980**, *102*, 6644.
(46) A detailed account of the analysis of the Mössbauer and magnetic susceptibility data and the accuracy of the determination of the zero-field splitting parameters will be given elsewhere. A table of the fine and hyperfine parameters of the $[L_2FeS_2MS_2]^{2-}$ complexes has been deposited as supplementary material.

Table VI. Mössbauer and Magnetic Susceptibility Parameters of the $[L_2FeS_2MS_2]^{2-}$ Complexes[a]

	temp, K							
	300		77		4.2		4.2	300
complex	IS,[b] mm/s	QS, mm/s	IS,[b] mm/s	QS, mm/s	IS,[b] mm/s	QS, mm/s	μ_{eff}, μ_B	μ_{eff}, μ_B
$[(PhS)_2FeS_2MoS_2]^{2-}$	0.33 (1)	1.94 (1)	0.44 (1)	1.96 (1)	0.45 (1)	1.96 (1)	4.13 (6)	4.90 (5)
$[(PhS)_2FeS_2WS_2]^{2-}$	0.39 (1)	2.20 (1)	0.47 (1)	2.24 (1)	0.48 (1)	2.24 (1)	4.15 (6)	4.88 (2)
$[(S_5)FeS_2MoS_2]^{2-}$	0.38 (1)	1.43 (1)	0.47 (1)	1.45 (1)	0.49	1.40[d]	4.43 (6)	4.90 (2)
	0.22 (1)[c]	1.20 (2)[c]	0.38 (2)[c]	1.18 (2)[c]				
$[(S_5)FeS_2WS_2]^{2-}$	0.42 (1)	1.68 (1)	0.51 (1)	1.66 (1)	0.51	1.60[d]	4.16 (6)	4.90 (1)

complex	77 K IS,[b] mm/s	complex	77 K IS,[b] mm/s	complex	77 K IS,[b] mm/s	complex	77 K IS,[b] mm/s
$[(Cl)_2FeS_2MoS_2]^{2-}$[e]	0.59	$[(Cl_2Fe)S_2MoS_2(FeCl_2)]^{2-}$[f]	0.57	$[(PhS)_4Fe]^{2-}$[g]	0.64	$[(O_2C_2S_2)(PhS)_2Fe]^{2-}$[g]	0.64
$[(Cl)_2FeS_2WS_2]^{2-}$[e]	0.65	$[(Cl_2Fe)S_2WS_2(FeCl_2)]^{2-}$[f]	0.63	$[(O_2C_4S_2)_2Fe]^{2-}$[g]	0.63	$FeCl_4^{2-}$[h]	1.01

[a] All as the Ph_4P^+ "salts". [b] With respect to Fe at room temperature. [c] Due to the $[(S_6)FeS_2MoS_2]^{2-}$ minor component. [d] Magnetically perturbed spectra at 4.2 K were fitted with the major component only (see text). [e] Reference 7. [f] References 10 and 51. [g] Reference 49. [h] Reference 50.

in solid $(Et_4N)_2[(PhS)_2FeS_2MoS_2]$[11] is not apparent in the Mössbauer spectra of the Ph_4P^+ salts at the same temperature. The presence or absence of magnetic interactions may be related to differences in the intermolecular Fe–Fe distances in the two different lattices as discussed previously. The Mössbauer measurements for the two homologues in the solid state at 4.2, 77, and 300 K are very similar. Simple fits of these spectra give the parameters of the isomer shift (IS) and quadrupole splitting (QS) depicted in Table VI.

Zero-field splitting parameters (D and E) for the Fe ion can be determined also from the magnetically perturbed Mössbauer spectra. The Mössbauer spectra of the Mo and W complexes at low temperatures and tranverse magnetic fields (up to 6 T) are shown in Figure 5. The solid lines represent fits of these spectra according to the spin Hamiltonian

$$H_n = \langle\vec{S}\rangle\cdot\mathbf{A}\cdot\vec{I} + \frac{e^2qQ}{12}[3I_z^2 - {}^{15}/_4 + \eta(I_x^2 - I_y^2)] - g_n\beta_n\vec{H}_{ext}\cdot\vec{I} \quad (2)$$

where $\langle\vec{S}\rangle$ is the expectation value of the electronic spin, $\vec{S}$, determined by diagonalization of the Hamiltonian H_e, $\mathbf{A}$ is the hyperfine constant tensor, I is the nuclear spin, and e^2qQ is the quadrupole interaction constant. Equation 2 is written in the electric field gradient system, which is related with the coordinate system of the Hamiltonian (1) through the Euler angles α, β, γ. The parameters determined by the fit have been deposited as supplementary material. The simulation of the magnetically perturbed spectra with the Hamiltonians (1) and (2) was not possible in the case of small external fields due to intermediate spin-relaxation effects. Analysis with spin-relaxation theories[46] showed that the electronic spin relaxation is faster for the Mo complex than for the W homologue.

(b) $[Ph_4P]_2[(S_5)FeS_2MS_2]$ (M = Mo, W). The magnetic susceptibility data for these complexes are similar to those depicted in Figure 4, and the corresponding parameters are also similar.[46] The Mössbauer spectra at 78 and 4.2 K for the Mo and W complexes are shown in Figure 6. At 4.2 K, magnetic hyperfine interactions are apparent. These interactions, which are already present at $T = 10$ K, are enhanced at lower temperatures. These interactions, very likely, are due to long-range magnetic order, and they are not observed in samples diluted in DMF. This ordering, very likely, is facilitated by the layer structure of the $[(Ph_4P)_2][S_5FeS_2MS_2]$ lattices (Figure 3), where anion layers alternate with cation layers.

In the 77 K spectrum of the Mo complex a second component is evident (Figure 6) by the asymmetry of the positive-velocity peak. The spectrum can be analyzed in terms

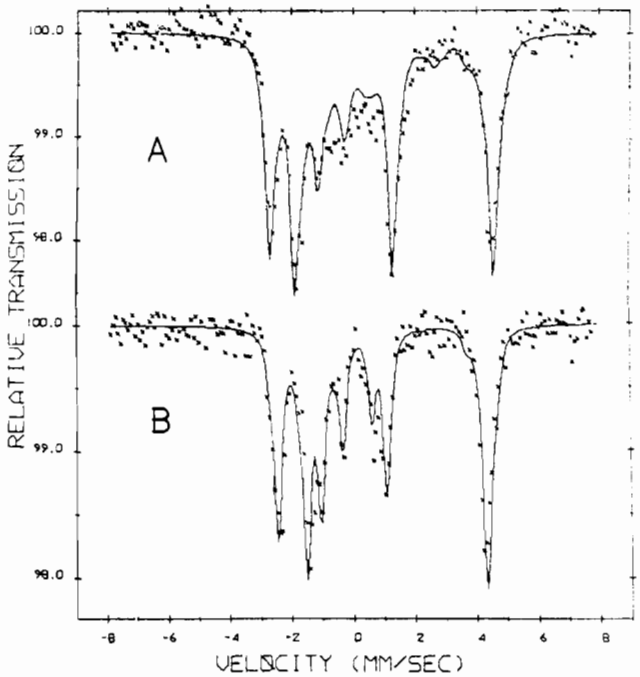

Figure 5. Mössbauer spectra of the $[(PhS)_2FeS_2MS_2]^{2-}$ complexes at 4.2 K and 2.0 T transverse magnetic field for M = Mo (A) and M = W (B). Solid lines represent least-squares fits of the experimental data.

of two components with an intensity ratio of ~3/1. This ratio does not change appreciably as a function of temperature and does not represent a spin equilibrium mixture for the two components.[47] The appearance of the minor component in dilute frozen solution samples as well suggests that the sample contains two different molecular species. This suggestion is substantiated by the X-ray structure determination results, which show the $[(S_6)FeS_2MoS_2]^{2-}$ complex occupying the $[(S_5)FeS_2MoS_2]^{2-}$ lattice site as a minor component with a ~0.3 occupancy factor.

The spectra of the two homologues at 4.2 K and in the presence of an external field of 0.9 T very roughly resemble those shown in Figure 5 and have been fitted in the limit of slow spin relaxation according to Hamiltonians (1) and (2). For both of these complexes the electron spin has achieved its saturation value. In this analysis the molecular field has been neglected since it is small (~0.1 T) with respect to the ex-

(47) Gütlich, P.; Link, R.; Trautwein, A. In "Mössbauer Spectroscopy and Transition Metal Chemistry"; Springer-Verlag: New York, 1978; p 100.

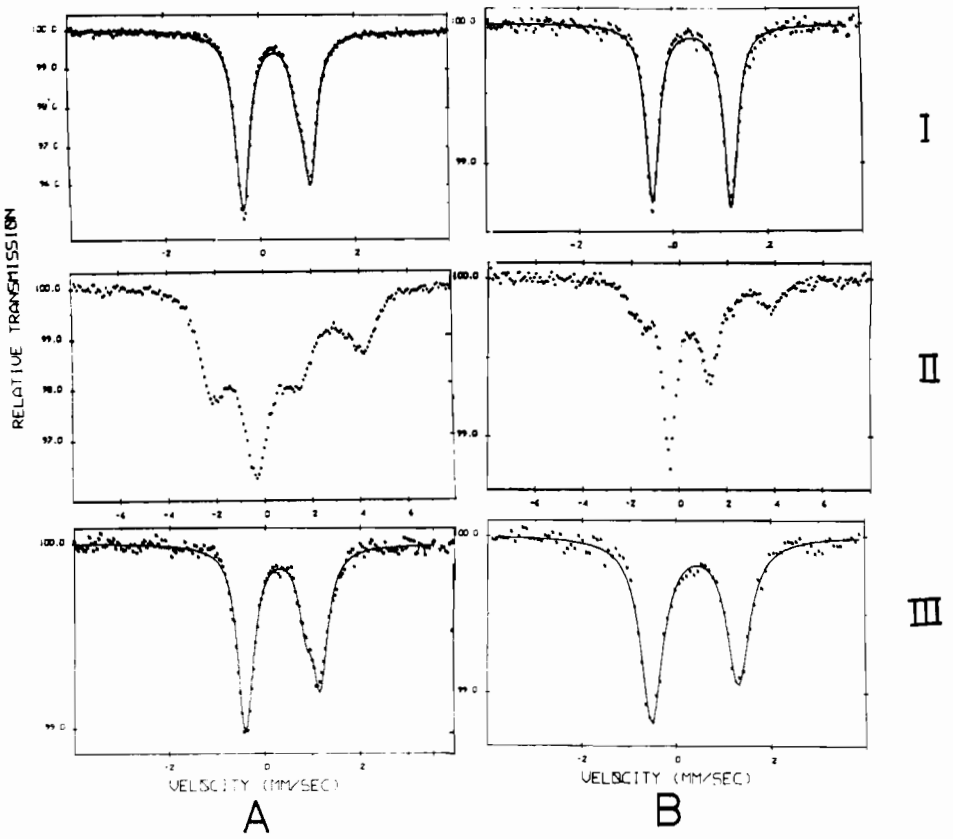

Figure 6. Mössbauer spectra of the $[(S_5)FeS_2MS_2]^{2-}$ complexes for M = Mo (A) and M = W (B) taken as powder spectra at 78 (I) and 4.2 K (II) and frozen DMF solution spectra at 4.2 K (III). Solid lines represent least-squares fits of the experimental data.

ternally applied magnetic field. The second site of the Mo complex is not easily discernible in the magnetically perturbed spectrum, presumably because of its low intensity and the spread of the magnetically split spectrum (an indication of extra absorption is noticeable at ~ -3 mm/s).

Discussion of the Mössbauer and Magnetic Susceptibility Data. The analyses of the data have been based on the assumption that the formal oxidation state of Fe in all the complexes is +2. This assumption is supported by the saturation magnetic effective moment, μ_{eff}, which is in excellent agreement with the spin-only value of ferrous ion ($\mu_{eff} = 4.9$ μ_B). A close examination of the Mössbauer parameters reveals substantial differences among the examined analogues, which display a variation of the electronic charge distribution in these systems. The parameter that is more directly related to the electronic charge at the iron site is the isomer shift. Despite several exceptions, it is firmly established that a decrease in the population of d-type orbitals results in a decrease of the isomer shift.[48] The isomer shifts of the complexes reported herein as well as of some other binuclear and trinuclear Fe–S_2MS_2 complexes are shown in Table VI. In the same table are included for comparison the isomer shifts of tetrahedrally coordinated Fe(II) either by chloride ions or by sulfur-containing ligands. An inspection of the data clearly shows that a replacement of two thiophenolate ligands (or the $S_2C_4O_2^{2-}$ chelate) by the MS_4^{2-} (M = Mo, W) ligands results in a decrease of the isomer shift by 0.2 mm/s. A similar effect is observed with the Cl^- ligands as well. Thus, replacement of two Cl^- ions by the MS_4^{2-} groups results in an isomer shift decrease of ~ 0.4 mm/s. This correlation aptly illustrates the strong electron delocalization from the iron toward the MS_4^{2-} ligands. A small but systematic increase in the isomer shift, by ~ 0.04 mm/s, is observed for the WS_4^{2-} complexes when compared to the values for their Mo analogues. The larger values of the isomer shifts for the iron sites in the WS_4^{2-} complexes reflects the somewhat reduced effectiveness of these anions to accept charge. The weaker Fe–WS_4 interactions apparent in the structural parameters of the Fe–S_2WS_2 units and the more negative reduction potentials observed for the Fe–WS_4 complexes (vide infra) are in concert with the Mössbauer results.

Of some interest are the Mössbauer parameters observed for the $[(S_6)FeS_2MoS_2]^{2-}$ minor component in the $(Ph_4P)_2$-$[(S_5)FeS_2MoS_2]$ samples. The isomer shift and quadrupole splitting parameters of this component indicate a "more ferric" valence state (Table VI). However, the saturation effective magnetic moment of the "mixed-anion" salt is equal to the spin-only value for a ferrous ion (Table VI). These results suggest that the enhanced electron delocalization observed for the minor component is still too small to affect the spin and therefore the magnetic moment of the iron. An alternative explanation could be one that assumes complete charge transfer and describes the FeS_2Mo unit as a Fe(III)–Mo(V)-coupled unit. With the assumption of a strong antiferromagnetic coupling in such a unit between Fe(III) ($S = {}^5/_2$) and Mo(V) ($S = {}^1/_2$), an $S = 2$ ground state can be realized in agreement with the observed effective magnetic moment.[30]

The electronic parameters[46] derived by both the magnetic susceptibility and the Mössbauer data show that in all cases the zero-field splitting D is negative. This corresponds to an easy direction of magnetization along the z axis of the **D** tensor which, as derived by the analysis,[46] nearly coincides with the z axis of the electric field gradient (EFG) system. The small

(48) Walker, L. R.; Werthein, G. K.; Jaccarino, V. *Phys. Rev. Lett.* **1981**, *6*, 98.
(49) Kostikas, A.; Petrouleas, V.; Simopoulos, A.; Coucouvanis, D.; Holah, D. G. *Chem. Phys. Lett.* **1976**, *38*, 582.
(50) Edwards, P. R.; Johnson, C. E.; Williams, R. J. P. *J. Chem. Phys.* **1967**, *47*, 2074.
(51) Simopoulos, A.; Papaefthymiou, V.; Kostikas, A.; Petrouleas, V.; Coucouvanis, D.; Simhon, E. D.; Stremple, P. *Chem. Phys. Lett.* **1981**, *81*, 261.

Table VII. Electronic Spectra of the Fe-M-S Complexes (M = Mo, W)

complex	λ_{max} (ϵ), nm			
	region A	region B	region C	other
$[(SPh)_2FeS_2MoS_2]^{2-}$	960 (sh)	620 (sh)	487 (8640)	
	865 (~115)	550 (sh)	425 (7770)	
$[(SPh)_2FeS_2WS_2]^{2-}$	1125 (sh)	540 (sh)	432 (4400)	
	900 (sh)	466 (sh)	362 (5500)	
$[(S_5)FeS_2MoS_2]^{2-}$	1125 (sh)	605 (1860)	480 (7240)	305 (14 890)
	900 (sh)	545 (sh)	410 (9920)	
$[(S_5)FeS_2WS_2]^{2-}$	1200 (115)	550 (1100)	425 (6000)	319 (13 870)
	963 (165)	464 (sh)	366 (7800)	

variation of the zero-field parameters and the hyperfine tensor components are within the uncertainties of the analysis and cannot be discussed with respect to the molecular geometry and charge distribution of the complexes.

Interesting magnetic effects are apparent from the low-temperature Mössbauer and magnetic susceptibility measurements on the Fe–MS_4 complexes. The $(Ph_4P)_2[(PhS)_2FeS_2MS_2]^{2-}$ complexes (M = Mo, W) remain paramagnetic at temperatures as low as 1.2 K. By contrast the Et_4N^+ salt of the Mo complex shows magnetic ordering at temperatures lower than 35 K.[11] These differences suggest that the molecular packing in the Et_4N^+ salt provides effective pathways for superexchange interactions appropriate for long-range magnetic ordering. A comparison of the Fe–Fe intramolecular distances, in the lattices of the Et_4N^+ and Ph_4P^+ salts, show that the closest Fe–Fe distances in the former are ~1.5 Å shorter than those in the latter. The difference in packing forces may also be responsible for the smaller quadrupole interaction observed[11] for the Et_4N^+ salt (M = Mo, ΔEq = 1.73 mm/s), by comparison to that for the Ph_4P^+ salt (Table VI).

The $(Ph_4P)_2[(S_5)FeS_2MS_2]$ complexes show magnetic hyperfine splitting at zero magnetic field in powder samples. This splitting is absent in frozen DMF solutions. This behavior is indicative of intermolecular magnetic coupling in the solid state leading to magnetic order. The magnetic susceptibility data however display paramagnetic behavior to temperatures as low as 2 K. This discrepancy may be due to low-dimensional magnetic ordering that is not clearly manifested in the magnetization data of powder samples in the region of rapid increase of the susceptibility. The crystallographic data in fact show an alternating, two-dimensional packing of the cations and anions which would support a low-dimensional ordering (Figure 3).

Electronic Spectra. The electronic spectra of the Fe–M–S complexes in the visible and near-infrared regions are characterized by absorptions that can be separated into three different groups (regions A–C, Table VII). A hypsochromic shift of the absorptions in regions B and C (Figure 7) are observed for the W complexes when compared to the Mo analogues. The energies of the two intense absorptions observed in region C for the Mo and W complexes have mean values that are very close to the energy of the S → M ($\pi(t_1)$ → d(e)) transition in the MS_4^{2-} anions.[31] The latter transition is observed at 470 and 392 nm in MoS_4^{2-} and WS_4^{2-}, respectively.[1c] It appears that the MS_4^{2-} S → M transition is split in the Fe–MS_4 complexes due to the lowering in local symmetry of the coordinated MS_4^{2-} units to C_{2v}. The absorptions in region C therefore must be attributed to S → M transitions.

The absorptions observed in region B are assigned to primarily S → Fe charge-transfer transitions since no such low-energy absorptions are observed in the spectra of the MS_4^{2-} anions. As noted previously[7] a unique feature in the near-infrared reflectance and solution electronic spectra of the Fe–MS_4 complexes is a broad absorption band with considerable structure centered around 1000 nm (region A, Table VII). This absorption tentatively is assigned to Fe → M transitions.

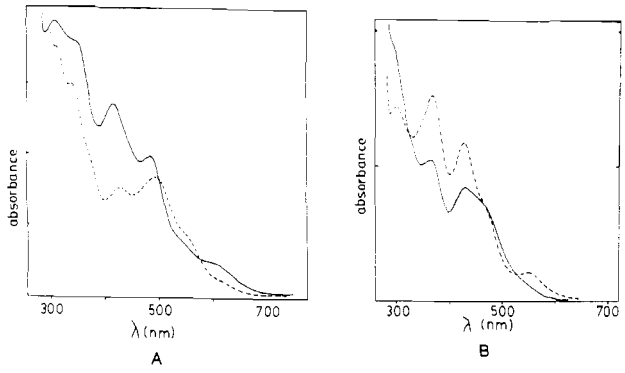

Figure 7. Visible spectra of (A) $[(PhS)_2FeS_2MoS_2]^{2-}$ (---) and $[S_5FeS_2MoS_2]^{2-}$ (—) and (B) $[(PhS)_2FeS_2WS_2]^{2-}$ (—) and $[S_5FeS_2WS_2]^{2-}$ (---) in DMF solution (Table VII).

Absorptions similar to those observed for the $[(S_5)FeS_2MoS_2]^{2-}$ and $[(PhS)_2FeS_2MoS_2]^{2-}$ anions are observed also in the electronic spectra of the $[(Gly)_2(Gly_2\text{-}Cys)_2]FeMoS_4$ and $(Gly)_2(Gly_2\text{-}Cys)_4Fe_2(MoS_4)_2$ peptide complexes.[52] A tentative MO scheme that qualitatively attempts to explain the spectral properties of the Fe–S_2MS_2 complexes has been suggested.[7] In this scheme the Fe d orbitals are placed between the empty M(VI) d orbitals and the primarily S MO's of the MS_4^{2-} thioanions.

The complexity as well as the predictability in the spectral patterns of the Fe–S_2MS_2 complexes suggests that the electronic solution spectra could be used as diagnostic criteria for the presence of the Fe–S_2MS_2 chromophores in other systems. Similarities to the spectra of $[(S_5)FeS_2MoS_2]^{2-}$ and $[(Gly)_2(Gly_2\text{-}Cys)_2]FeS_2MoS_2$ complexes in regions B and C (Table VII) are apparent in the electronic solution spectra of acid–base-treated nitrogenase solutions[53] and of the Fe–Mo protein isolated from *Desulfovibrio gigas*.[54] The possibility that Fe–S_2MoS_2 chromophores exist at least in acid–base-treated nitrogenase solutions is supported by the chromatographic separation of MoS_4^{2-} from such solutions.[53]

Electrochemical Studies. The voltammograms for the $[(PhS)_2FeS_2MS_2]^{2-}$ and $[(S_5)FeS_2MS_2]^{2-}$ complexes are quite complex and display a number of oxidation and reduction waves, all of which are irreversible. The peak potentials for all waves are shown in Table VIII. For all of the complexes a new wave appears at about −0.6 V in the cathodic scan when the anodic scan is performed first. When the electrode surface is clean and when the cathodic scan is performed first, no wave is observed at −0.6 V. The reduction at −0.6 V very likely involves a common ligand oxidation product generated in the anodic scan.

(52) Balasubramanian, A.; Coucouvanis, D. *Inorg. Chim. Acta* **1982**, *66*, L65.
(53) Zumft, W. G. *Eur. J. Biochem.* **1978**, *91*, 354.
(54) Moura, J. J.; Xavier, A. V.; Bruschi, M.; Legall, J.; Cabral, J. M. P., *J. Less-Common Met.* **1977**, *54*, 555.

Table VIII. Voltammetric Data for the $L_2FeS_2MS_2$ Complexes

complex	$E_{p,c}{}^a$ ($i_p/v^{1/2}c$)^b	$E_{p,a}{}^c$ ($i_p/v^{1/2}c$)
$(Ph_4P)_2[(PhS)_2FeS_2MoS_2]$	−1.19 (96), −1.49 (125)	0.20 (22), 0.52 (162), 0.66 (160)
$(Ph_4P)_2[(PhS)_2FeS_2WS_2]$	−1.67 (94), −1.91 (306)	0.20 (94), 0.56 (282), 0.84 (440)
$(Ph_4P)_2[(S_5)FeS_2MoS_2]$	−1.50 (77), −1.84 (266), −1.91 (293)	0.42 (162), 0.60 (139), 1.36 (177)
$(Ph_4P)_2[(S_5)FeS_2WS_2]$	−1.56 (63), −1.82 (190), −1.89 (218)	0.44 (101), 0.70 (60), 1.38 (348)

^{a} $E_{initial} = -0.2$ V vs. SCE; the initial scan direction is negative. ^{b} i_p = peak current; c = concentration. For a one-electron process, reversible electron transfer, $i_p/v^{1/2}c = 35$ μA $(v/s)^{-1/2}$ mM. ^{c} $E_{initial} = -0.2$ V vs. SCE; the initial scan direction is positive.

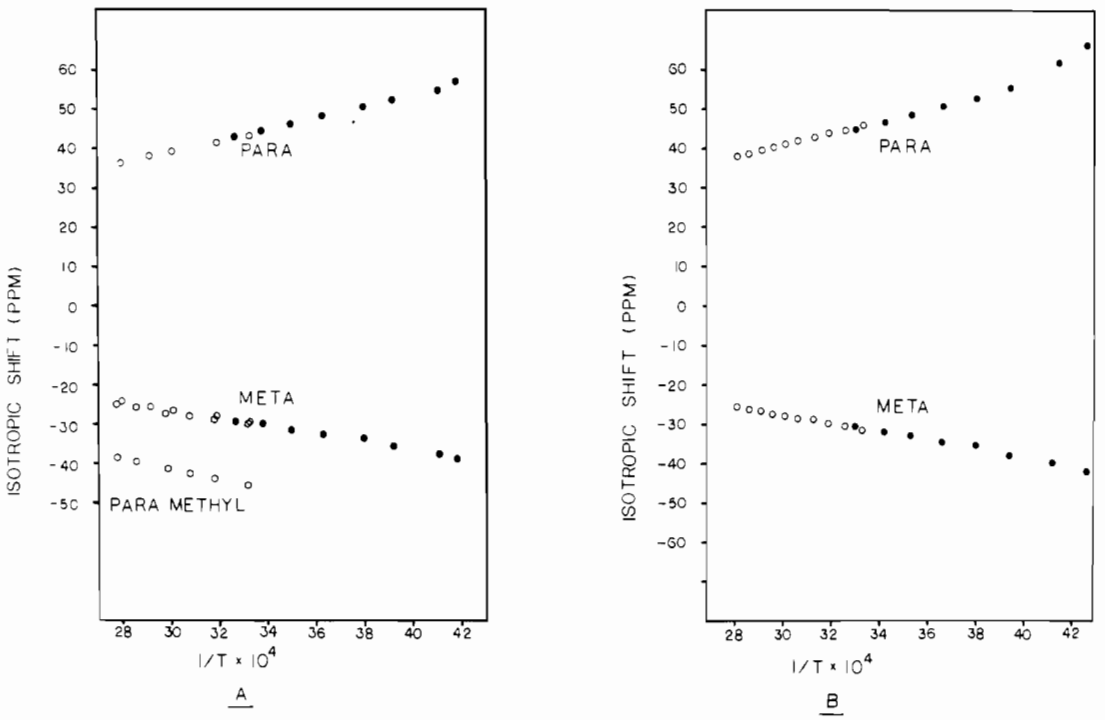

Figure 8. Temperature dependence of isotropic shifts $(\Delta H/H_0)_{iso}$ in ppm of (A) $[(Ph_4P)_2][(PhS)_2FeS_2WS_2]$ in CD_3CN (●) and Me_2SO-d_6 (○) and $[(Ph_4P)_2][(p\text{-}CH_3PhS)_2FeS_2WS_2]$ in Me_2SO-d_6 (○) and (B) $(Et_4N)_2[(PhS)_2FeS_2MoS_2]$ in CD_3CN (●) and Me_2SO-d_6 (○).

An examination of the voltammetric waves of the $[(PhS)_2FeS_2MS_2]^{2-}$ complexes (Table VIII) leads to the following conclusions: (a) With the exception of the anodic wave at +0.20 V all other waves correspond to multielectron diffusion-controlled processes. (b) The peak potentials for the two reduction waves are strongly dependent on the identity of M (Mo vs. W). (c) The three oxidation waves are only slightly affected by the identity of M (Mo vs. W).

The first conclusion is based on the values for the peak current function $i_p/v^{1/2}c$, which in DMF solution and on a Pt electrode should be[55] in the range of 32–35 μA $(V/s)^{1/2}$ mM. With the exception of the oxidation wave at +0.20 V all other waves show peak current functions much larger than expected (Table VIII). The two reduction waves are found at values 480 and 420 mV more negative for the W complex than for the corresponding Mo complex. This behavior suggests that the site of reduction is centered on the MS_4^{2-} anions. The relative potentials of these reductions are consistent with the greater oxidizing strength of Mo(VI) compared to that of W(VI) and with the greater ability of the MoS_4^{2-} anions to accept electrons from Fe(II) in the $[(PhS)_2FeS_2MoS_2]^{2-}$ complexes.

The small shifts in the three oxidation waves by 0, 40, and 180 mV from Mo to W, and a shift (for the third wave) in a direction opposite to that expected for the replacement of Mo with W, suggest that the rate-limiting steps in the oxidation processes involve ligand oxidations.

The voltammetry of the $[(S_5)FeS_2MS_2]^{2-}$ complexes shows virtually identical waves for either Mo or W (Table VIII). This independence from the MS_4^{2-} ligand suggests that the voltammetric waves are associated primarily with the FeS_5 unit. As with the $[(PhS)_2FeS_2MS_2]^{2-}$ complexes all of the redox waves involve multielectron diffusion-controlled processes.

^{1}H NMR Spectra of the $[(C_6H_5)_4P]_2[(C_6H_5S)_2FeS_2MS_2]$ Complexes. The ^{1}H nuclear magnetic resonance spectra of these complexes were recorded as a function of temperature, in both CD_3CN and deuterated dimethyl sulfoxide (Me_2SO-d_6) solutions. The $(C_6H_5)_4P^+$ cation resonances were observed at their normal positions and were only slightly broadened and shifted relative to the corresponding resonances in diamagnetic $(C_6H_5)_4PCl$ solutions.

The C_6H_5S proton resonances were broadened significantly and were shifted greatly upfield and downfield from Me_4Si. At a temperature of 298 K, resonances were observed downfield from Me_4Si at −37.5 ppm for M = Mo and at −36.6 ppm for M = W. At the same temperature resonances upfield from Me_4Si were observed at +37.8 ppm for M = Mo and at +35.9 ppm for M = W.

The downfield resonances were, approximately, twice as intense as the upfield resonances and were assigned to isotropically shifted meta protons. The less intense upfield resonances were assigned to the isotropically shifted para protons. These assignments were confirmed by an examination of the ^{1}H NMR spectra of the p-$CH_3C_6H_4S$ analogue complexes. No upfield resonances were observed in the spectra of these complexes, and a new downfield resonance emerged

(55) Nicholson, R. S.; Shain, I. *Anal. Chem.* **1964**, *36*, 706.

Table IX. Isotropic[a] Shifts of Proton Resonances in the $(ArS)_2FeS_2MS_2$ Complexes at 298 K

complex	$(\Delta H/H_0)_{iso}$, ppm: *m*-H	*p*-H, $-CH_3$	solvent
$(C_6H_5S)_2FeS_2MoS_2^{2-}$	−31.1	45.9	Me_2SO-d_6
	−30.3	45.0	CD_3CN
$(CH_3C_6H_4S)_2FeS_2MoS_2^{2-}$	−28.9	−48.0	CD_3CN
$(C_6H_5S)_2FeS_2WS_2^{2-}$	−27.8	43.2	Me_2SO-d_6
	−29.8	−45.5	CD_3CN
$(CH_3C_6H_4S)_2FeS_2WS_2^{2-}$ [b]	−29.8	−45.5	CD_3CN

[a] $(\Delta H/H_0)_{iso} = (\Delta H/H_0)_{obsd} - (\Delta H/H_0)_{dia}$. Diamagnetic corrections for the free ligands were taken from ref 57a. [b] $T = 304$ K.

at −50.2 ppm for M = Mo and at −47.7 ppm for M = W. The assignment of the new downfield resonances to the isotropically shifted *p*-CH_3 protons is supported by the approximate 3/2 relative integrated intensity ratio of the two downfield resonances. The ortho-proton resonances were not detected unequivocally and probably have been broadened beyond recognition.

Isotropic shifts in paramagnetic molecules can be the result of Fermi contact and dipolar (pseudocontact) interactions.[56] In the absence of dipolar contributions the isotropic shift is the result of contact interactions and is proportional to the magnetic susceptibility at the same temperature. The lack of attenuation of the isotropic shifts (of the C_6H_5S protons in the $[(C_6H_5S)_2FeS_2MS_2]^{2-}$ complexes), as the distance of the protons from the paramagnetic metal center increases, suggests that the observed isotropic shifts are primarily Fermi contact in nature. This conclusion is further supported by the observed alternation of sign for the shifted proton resonances. This sign alternation is diagnostic of contact shifts by a π spin delocalization mechanism.[56] The isotropic shifts of the proton resonances in the phenylthiolate ligands have been studied thoroughly in other systems.[57]

The isotropic shifts of the coordinated thiophenolate ligand protons, relative to those for the corresponding protons in the free thiols, are listed in Table IX (T = 298 K). The magnitudes of the isotropic shifts decrease with increasing temperature in the temperature range from −40 to +80 °C. Plots of $(\Delta H/H_0)_{obsd} - (\Delta H/H_0)_{dia}$[58] vs. T^{-1} for the Mo and W complexes in CD_3CN or Me_2SO-d_6 solutions (Figure 8) show (a) no appreciable solvent effects in the isotropic shifts and (b) slightly larger shifts for the Mo complexes by comparison to those signals for the W analogues. The second observation is consistent with the more "ferric" character of the iron in the Mo complexes apparent from the Mössbauer isomer shift data (Table VI). The nearly straight-line relationship of the isotropic shift vs. T^{-1} (Figure 8) is indicative of magnetic behavior that follows the Curie law.[59] This result, which is consistent with the magnetic susceptibility studies, rules out the population of higher energy magnetic states at temperatures as high as 350 K.

Summary. The MS_4^{2-} anions coordinate readily to Fe(II), and dinuclear $[L_2FeS_2MS_2]^{2-}$ complexes are obtained that contain the FeS_2M unit as a common structural feature. This rhombic unit is nearly planar and is characterized by acute Fe–S–M angles (~74°) and rather short Fe–M distances of ~2.74 Å.

The FeS_4 units in the $[(PhS)_2FeS_2MS_2]^{2-}$ complex anions, in two different lattices, show pronounced distortions from tetrahedral geometry. These distortions are explained in terms of specific intramolecular interactions. Distortions of equal magnitude are observed also in the FeS_4 units of the $[(S_5)FeS_2MS_2]^{2-}$ complexes. These distortions are tentatively attributed to crystal packing forces. The Fe–S bond lengths in the FeS_4 units of all complexes are somewhat shorter than expected for a $Fe^{II}S_4$ chromophore. A parallel lenghtening of the M–S bond lengths is found in the MS_4^{2-} thioanions upon coordination to iron. These structural data and, more definitively, the ^{57}Fe Mössbauer isomer shift values indicate considerable Fe → MS_4 charge transfer, which results in partial oxidation of the Fe(II) ions and partial reduction of the MS_4^{2-} ligands in the Fe–MS_4 complexes. The extent of charge transfer is slightly less pronounced in the WS_4^{2-} complexes and correlates with the weaker oxidizing potential of the WS_4^{2-} anion. The ability of the MS_4^{2-} anions to delocalize charge in the Fe–MS_4 complexes very likely derives from the availability of low-lying unoccupied M d orbitals in the coordinated MS_4^{2-} anions.

The rhombic FeS_2Mo unit in the $[L_2FeS_2MoS_2]^{2-}$ complexes may well represent a feature of structural importance in the Fe–Mo–S aggregate of nitrogenase.

Acknowledgment. Financial support from the National Science Foundation (Grant No. CHE-79-0389), the National Institutes of Health (Grant No. GM 26671-02), and a NATO Research Grant (No. 1321) is gratefully acknowledged. The authors also wish to thank Professor M. Ryan for assistance with the electrochemical studies.

Registry No. $(Ph_4P)_2[(PhS)_2FeS_2MoS_2]$, 83602-17-9; $(Et_4N)_2[(PhS)_2FeS_2MoS_2]$, 72089-28-2; $(Ph_4P)_2[S_5FeS_2MoS_2]\cdot{}^1/_2DMF$, 83560-83-2; $(Ph_4P)_2[(PhS)_2FeS_2WS_2]$, 73493-04-6; $(Et_4N)_2[(PhS)_2FeS_2WS_2]$, 73493-05-7; $(Ph_4P)_2[S_5FeS_2WS_2]\cdot{}^1/_2DMF$, 83560-84-3; $(Ph_4P)_2[Fe(SPh)_4]$, 57763-34-5; $(NH_4)_2MoS_4$, 15060-55-6; $(Et_4N)_2[Fe(SPh)_4]$, 77403-03-3; $(NH_4)_2WS_4$, 13862-78-7.

Supplementary Material Available: Listings of atomic positional and thermal parameters for $(Ph_4P)_2[(S_5)FeS_2WS_2]$ (Table IVS), hydrogen atom positional and thermal parameters for all structures, calculated and observed structure factors for all four structures, fine and hyperfine parameters of the $[L_2FeS_2MS_2]^{2-}$ complexes as derived by the detailed analysis of the Mössbauer spectra, and angular distortions and intramolecular H contacts of the FeS_4 units in the C_2-$[(PhS)_2FeS_2MS_2]$ lattices and packing diagrams for $[(C_5H_5)_4N]_2[(PhS)_2FeS_2WS_2]$ and $[(C_6H_5)_4P]_2[(PhS)_2FeS_2MoS_2]$ (93 pages). Ordering information is available on any current masthead page.

(56) Horrocks, W. D. In "NMR of Paramagnetic Molecules"; LaMar, G. N., Horrocks, W. D., Holm, R. H., Eds.; Academic Press: New York, 1973.

(57) (a) Holm, R. H.; Phillips, W. D.; Averill, B. A.; Mayerle, J. J.; Herskovitz, T. *J. Am. Chem. Soc.* **1974**, *96*, 2109. (b) Reynolds, J. R.; Laskowski, E. S.; Holm, R. H. *Ibid. 1978*, **100**, 5315.

(58) Diamagnetic corrections for the ligands employed in Me_2SO-d_6 and CD_3CN were those measured previously.[57a]

(59) Jesson, J. P. In ref 56.